# Finite Element Approach to Photoemission of Complex Molecules

Tobias Möhle

November 30, 2016

# Contents

Notation:

- vectors: $\boldsymbol{r}$
- matrices: $\mathbb{R}$
- initial state: $\Psi_i$, final state: $\Psi_f$, single states/orbitals: $\Phi$ or $\Psi$; the dyson orbital in particlular:$\Phi_{\mathrm{DO}}$, ansatz functions $\phi$
- anihilition/creation operators: $\hat{a}$, $\hat{a}^\dagger$.
- spacial coordinates: $\boldsymbol{r}$, spin + coordinates: $\boldsymbol{x}$.

Abbreviations:

- CAP complex absorbing potential
- CI configuration interaction
- DO Dyson orbital
- DFT density functional theory
- DVR discrete variable approximation
- eV electron volt
- FD finite difference
- FEF free electron function
- FEM finite element method
- FE-DVR finite element discrete variable approximation
- GASCI
- FV finite volume
- LCAO linear combination of atomic orbitals
- RBF radial basis function
- SCF self-consistent field
- SD Slater determinant
- SA sudden approximation
- SE Schrödinger equation
- TDDFT time dependent density functional theory

# 1 | Introduction

Steady state as well as time-resolved photoelectron spectroscopy have become widely used tools to study the composition of gases and liquids [1–3], the structure of solids [4] as well as chemical reactions such as electron transfer [3]. The process studied by photoelectron spectra is the absorption of a high-energetic photon (usually in the ultra-violet to hard X-ray regime) by an $N$-electron system which leads to the releas of an electron whose kinetic energy is measured. This process is sketched in Figure 1.1 where the bound states are depicted by horizontal bars and the states of the outgoing electron are visualised by the gradient-filled block, indicating that its energy is continuous. Measureing the kinetic energy of the photoelectron yields information on the energy of its previous states due to energy-conservation over the process.

One of the main reasons for the broad success of this particular type of spectroscopy is that these spectra are very sensitive to small changes in the chemical environment and hence yield information not only about the chemical structure of molecules but also about intermolecular interactions as for example solvation effects [1, 5–8]. Furthermore, photoelectron spectroscopy provides a more direct access to the energy levels than optical absorption and emission spectroscopy since the transition energies are obtained with respect to the vacuum level and no "dark" states occur due to different selection rules. Finally the ease of handling changed particles experimentally makes this method appealing and a good temporal resolution can be achieved by varying the path in the time of flight spectrometer. Moreover, besides its capabilities in steady state spectroscopy, photoelectron spectra are the standard tool to study attosecond physics due to the naturally high energy of the short pulses which ionise the systems under

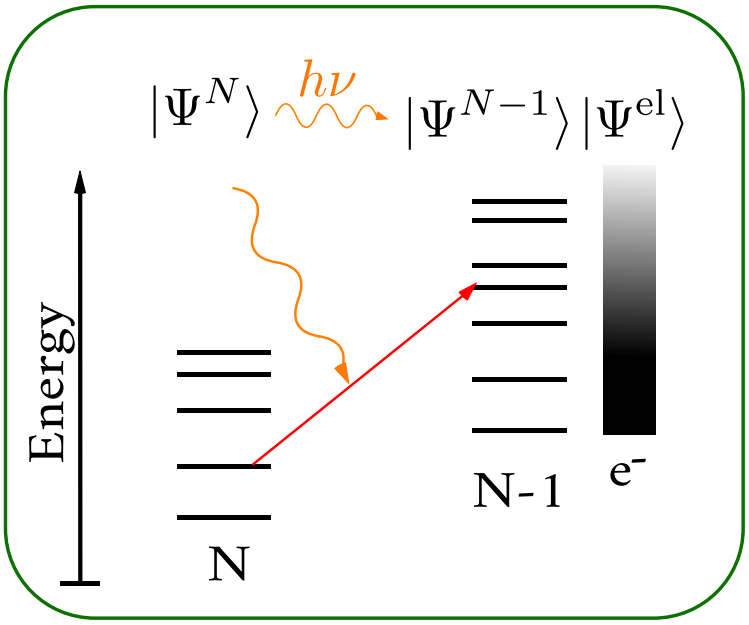


Figure 1.1: Schematic representation of a photoelctron transition : an incoming photon with energy $h\nu$ ionises the $N$-electron system, transfering it into a free electron in a continuum state and a system of $N-1$ bound electrons. The bars denote bound states, the color-gradient depicts the energy of the outgoing electron.

study [9–14]. However, a limitation of photoelectron spectroscopy is that the short free-path of electrons in condensed phases limits the probe depth significantly.

Having performed a measurement of a photoelectron spectrum (PES) it is, at least for complex systems, rich of features and hence the interpretation requires theoretical methods. This especially applies to systems with strong electron correlation which manifests itself in the appearance of combination transitions. Over the decades a large variety of methods to calculate photoelectron spectra have been developed at different levels of theory. In literature often the theoretical spectra are estimated on the basis of Koopmans' theorem [15], (or its density functional theory (DFT) counterpart [16],) assuming equal intensities for all transitions [17–20]. Even though this is a quite successful approach for solid states [21, 22] and gives an easy interpretation, it is too simplistic in many cases since it neglects electron relaxation and correlation effects and hence may give an invalid picture as shown by Cederbaum *et al.* even for small systems such as various diatomics [23, 24]. Furthermore in this model no reliable information about intensities can be obtained. To retrieve quantitative transition strengths, more advanced models are needed. Since simulations in time-domain are very demanding they are only applied to small molecules, mainly to study strong-field effects such as high harmonic generation [10, 25–28] which can not be described in frequency-domain. In this thesis however the focus is on complex molecular systems and a wide range of kinetic energies, while more moderate field strengths should be applied. Hence frequency-domain methods derived from a perturbation theory with respect to the irradiating electromagnetic field are applicable here.

In this thesis, the PESs are calculated within the Dyson orbital (DO) formalism which is derived and explained in more detail. This formalism is based on Fermis' Golden Rule [29] and allows a reduction of the dipole moment matrix element from an $N$-electron integral to effective one-particle quantities. Thereby the initial state and the bound part of the final state are represented by a one-electron quantity denoted as DO. The other wave function entering the dipole moment operator is the free electron function (FEF). In this formalism electron relaxation and correlation effects between bound states of the unionised and ionised systems are included, allowing the description of combination transitions. Per contra, this formalism neglects the correlation of the outgoing electron with the ionic remainder and thus may neglect certain transitions [30].

Since the bound state wave functions can be obtained from standard quantum-chemical tools, the computation of the DO is straightforward even though technically demanding [31]. The computation of the FEF is in general not trivial since analytic solutions are known only for few special cases such as hydrogen-like atoms [32] and general basis sets as they are used for bound states are not available. Among others, three analytic expressions have been suggested, each based on an expansion of spherically symmetric functions in plane waves [33]. One of them is the spherical wave basis which is a set of solutions of the Schrödinger equation (SE) without any potential and hence is especially well-suited for photodetachment from negative ions, leaving systems in an uncharged state [33, 34]. The other two expansions are based on Coulomb waves which assume a Coulomb potential and hence are exact for the ionisation of hydrogen-like atoms [32]. Thereby one of them is an expansion in Coulomb waves for the given momentum vector $\boldsymbol{k}$ while the other is an asymptotic expression for Coulomb waves with vanishing momentum (Coulomb $|\boldsymbol{k}| = 0$).

The functions each are expanded in a series of increasing quantum numbers for angular momentum $l$ and its projection $m$. Since all three functions assume spherical symmetry of the potential, they are expected to give a good approximation to the real FEF for spherically symmetric systems only. Ionisation *e. g.* from a delocalised orbital of a linear molecule have a different symmetry and thus can be expected to be described only crudely by this approach. The effects due to lower molecular symmetry become especially important for low kinetic energies because the interaction with the ionic remainder becomes strong in this case.

To analyse the quality of a given expression for a FEF, it is instructive to study the intensity of a given transition as a function of kinetic energy. Such a study is examined in Figure 1.2, showing the intensity of the photoionisation transition from the highest occupied molecular orbital (HOMO) of water for different kinetic energies of the photoelectron, estimated with the above-mentioned expansions. The comparison shows that all three expansions yield different intensities for most transition energies. Besides leading a wrong wrong symmetry of the FEF, these expansions yiled even in the limit of infinite terms only a plane-wave, neglecting the ionic potential and hence are not asymptotically correct.

To overcome the restrictions in symmetry and kinetic energy of the photoelectron function, an explicit formulation is needed, taking the molecular electrostatic potential experienced by the outgoing electron into account. Assuming that the correlation between the FEF and the bound states of the ion is weak (which is a prerequisit for the DO formalism anyway), one can use the mean-field potential of the molecular remainder. This allows for obtaining the FEF from the one-electron SE with an appropriate potential and thus reduces the complexity compared to the exact case where a coupled $N$-electron equation needs to be solved, considerably.

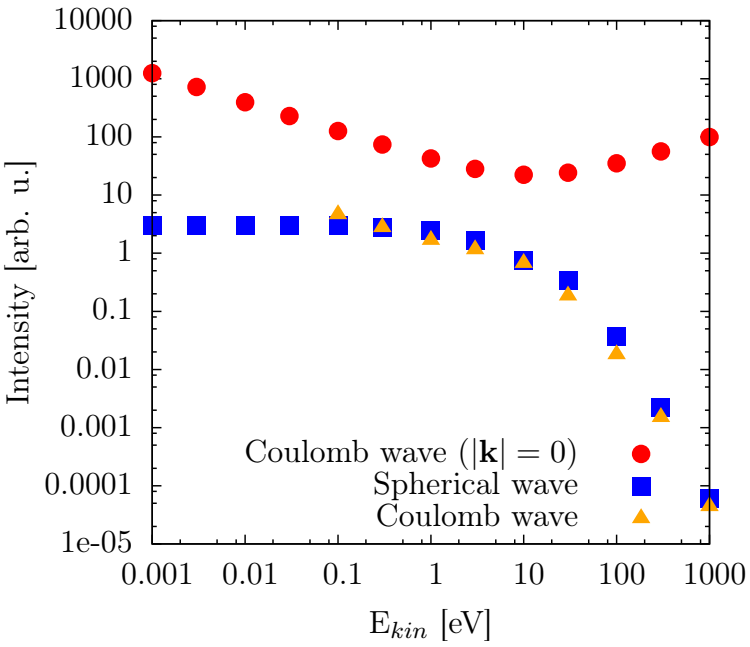


Figure 1.2: The intensity of the lowest-lying transition of water depending on the kinetic energy of the photoelectron. Each expansion is performed up to $l = 10$.

In the thesis at hand a good approximation to the FEF is aimed which should be applicable to a wide range of molecules and photon energies. Such a flexible description is possible exploiting the finite element method for solving the SE. In the finite element method, the space of interest is subdivided into small volume elements and solved variationally with stepwise polynomials whose support spans over one or few elements only [35, 36]. The finite element description is especially efficient here since the size of the elements

can be locally adapted to reproduce finer structures or broader shapes [35, 37]. Using finite elements, the one-particle SE is formulated a generalised eigenvalue problem with sparse matrices.

An important characteristic of the exact FEF is its spatially infinite extend which can not be handled by the finite element method. To describe the function in a good approximation, the finite elements are extended by infinite elements [38–41] which are volume elements with infinite radial extend that are connected to the outer surface of the finite element region. Thereby the radial function is a polynomial in $\frac{1}{r}$ multiplied by $e^{ikr}$, resembling the asymptotic behaviour of known analytic solutions and fulfilling the Sommerfeld radiation condition [42].

The bound states can be obtained on the level of density functional theory (DFT) which is a formally exact method based on the Hohenberg-Kohn theorem [43], stating that the total electron density determines all system properties such as electronic binding energies. However, the correct form of the exchange potential as well as the kinetic energy are not known as functionals of the electron densety and hence approximate functionals need used. While the kinetic energy can be estimated reasonably by the Kohn-Sham scheme [44], the expressions used for the exchange-correlation potential yield electron densities that have a wrong long-range asymptotic decay which affects the observables of these systems [18, 19, 45]. To reduce this error, range-separated hybrid functionals are used where the usual DFT exchange functionals are used at small distances while a Hartree-Fock exact exchange ensures the correct behaviour at larger distances. The interchange between these contributions is modelled via an error function with a characteristic distance that is optimized for each system separately. This procedure has been observed to enhance the accuracy of the predicted properties such as the orbital energies [45–48].

While the schemes described above are well established, their combination is only rarely used. Especially the FEF is found in literature to be approximated only crudely as plane-wave functions [49] or in some expansion as described above [31, 33, 46]. The goal of this thesis is to use the DO formalism with bound states being described by DFT using the above-mentioned optimized range-separated hybrid (OTRSH) functionals to obtain accurate orbital energies and complement it with a FEF that accounts the molecular electrostatic potential explicitly using the finite and infinite element methods which have been applied only to very few quantum mechanical problems [50, 51].

In the protocol used the DFT and time-dependent DFT calculations for excited states are done using a locally modified version of `NWChem` [52] and the `Gaussian 09` package [53]. From those, the DO is calculated with the in-house code `DYSON` developed previously [31]. A self-written interface extracts the required data as *e.g.* the molecular orbital coefficients and overlap matrix of atomic orbitals from the output of these programs. For the computation of the FEF, the implementation that is developed in the framework of this thesis uses the finite element library `Libmesh` [54]. It is an open source library that provides a broad range of capabilities and interfaces to several high-performance linear algebra libraries [55–57]. Moreover, it supports MPI parallelisation and implements a recent formulation of the above-mentioned infinite elements [41]. Especially the latter is to the best of my knowledge a unique option. Furthermore it has an automated procedure to adaptively refine or coarsen the elements according to local error estimates.

Tho goal of this thesis is to find a systematic way to setup the finite element mesh

for any given molecule to describe the photoelectron with a reasonable accuracy that goes beyond the capabilities of existing programs in this field. This procedure will be tested on different model systems.

- Lithium: light atomic system, many experimental and experimental reference data available, the `ezDyson` calculations are expected to give a good approximation.
- $CO_2$: linear easy molecule with some reference data available, used to test some further properties
- Benzene (?): More complex molecule with reference data, well investigated
- Some other system(s) for which `ezDyson` gives poor results (?)

# 2 The Calculation of Photoelectron spectra

The large variety of systems and effects studied with photoelectron spectroscopy lead to diverse methods [58, 59]. In this work the interest is in steady-state photoelectron spectra of molecular systems with a size up to some tens of atoms. As light source a classical ultra-violet or soft X-ray source is assumed as *e.g.* discharge lamps based on helium, hydrogen, mercury or similar gases.

However, besides this scenario, in the literature a large diversity of systems, studied with different inquests using photoelectron spectroscopy, is found. Hence a large variety of models for the description of the PES is available, differing in the numerical effort but also in the assumptions and approximations implied. These methods can be categorised as time- and frequency-domain approaches. As the Table 2.1 shows, the time-domain methods are restricted to small systems which is due to the fact that the $N$ electron problem needs to be solved for every time-step and hence several hundred times per simulation. In contrast to this, frequency-domain methods require only one solution and thus are much more efficient. However, the neglect of the nonlinear response properties make these schemes inappropriate when multiphoton ionisation and high harmonic generation (HHG) come into play.

Among the the frequency domain methods, the most prominent representative is the method denoted as Koopmans' approach in Table 2.1 [18, 60–62]. In this scheme, the systems ground state is computed with a given quantum mechanical method to obtain the electronic binding energies. The photoelectron spectrum is than estimated using the orbital energies as the transition energies and using uniform intensities. While this method has shown to be at qualitatively in good agreement with experiment for some systems [18, 19, 60, 63, 64], it breaks down in cases of strong electron correlation [23, 65] due to strong changes in the orbitals upon ionisation. This method is characterised by its

| | System Size | Typical Problems | Field Str. | QC | Formalism |
|---|---|---|---|---|---|
| Time-domain | atomic, diatomic, triatomic | HHG, Multiph. ionisation | strong | (TD)DFT, GASCI, CASSCF | Time-dep. DO SE |
| Frequency-domain | up to biomolecules | steady-state, time-res. PES, solid states, ... | weak | EOM-CC, RASSCF, TD-DFT | R-Matrix DO Greens' Function Koopmans' |

Table 2.1: Overview of the capabilities of time- and frequency-domain methods.

low computational costs and robustness and thus well-suited for very large systems such as solid states where calculations beyond ground-state DFT are very demanding on not feasible at all.

While in the Koopmans' approach only the ground state of the unionised state is considered, other methods treat the system under study in different ways. In Figure 2.1 the model of the system used the most important methods is schown schematically. In a similar way as the Koopmans' theorem takes only the initial state into account, the Greens' function approach is implicit on the photoelectron. A short introduction to this approach is given in section 2.1. Among those methods that treat all $N$ electrons both in the initial and final state is a large group of methods where the photoelectron is treated on the same footing. Out of this class, several approaches both in time- and frequency-domain are described in section 2.2. Finally the Dyson orbital formalism describes the full $N$-electron system in the final state but here the photoelectron is treated separately, neglecting correlation effects with the bound states. A more detailed derivation of the expressions used in this formalism is given in section 2.3.

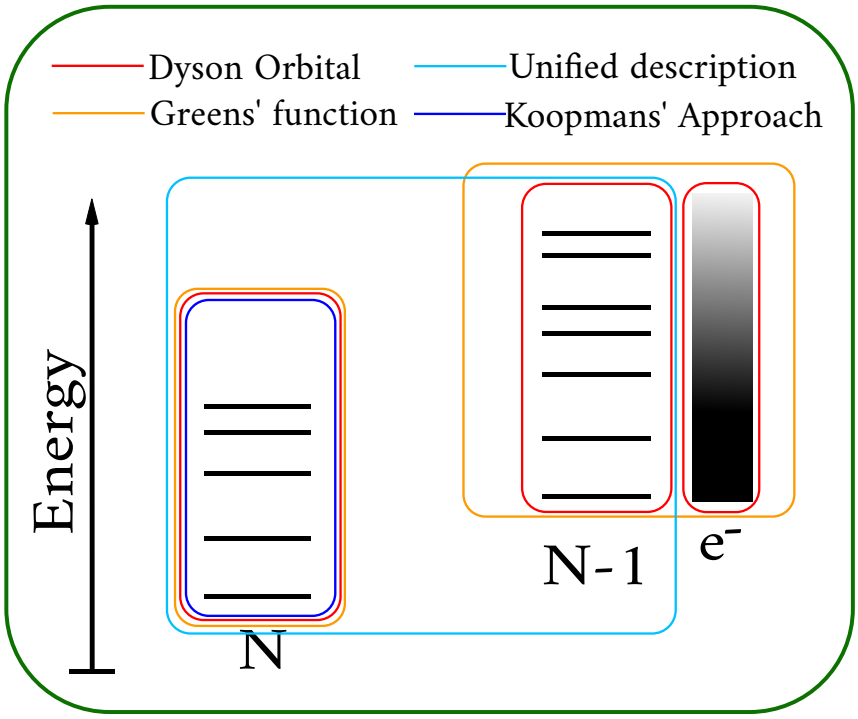


Figure 2.1: Scheme of the system-representation used in the different methods.

## 2.1 The Greens' Function Approach

In contrast to most other quantum-chemical methods, in the Greens' function approach expectation values for a given operator $\hat{O}$ are not computed as a scalar product $\langle\Psi^N|\hat{O}|\Psi^N\rangle$ with the wave function $|\Psi^N\rangle$ of the $N$ electron state of interest, but by contour integrals with the Greens' function [66, 67]. Thereby the (one particle) Greens' function is a matrix $\mathbb{G}$ whose elements are defined as

$$G_{j,k}(t,t') = -\mathrm{i}\langle\Psi^N|\hat{T}\left(\hat{a}_j(t)\hat{a}_k^\dagger(t')\right)|\Psi^N\rangle \tag{2.1}$$

with the creation operator $\hat{a}_j^\dagger(t) = e^{\mathrm{i}\hat{H}t}\hat{a}_j^\dagger e^{-\mathrm{i}\hat{H}t}$ of an electron in state $j$ at time $t$ in Heisenberg picture and the annihilation operator $\hat{a}(t) = e^{-\mathrm{i}\hat{H}t}\hat{a}_j e^{\mathrm{i}\hat{H}t}$ respectively. $\hat{T}$ denotes is the Dyson time ordering operator that orders the operators $\hat{a}$ and $\hat{a}^\dagger$ by their time arguments

to ensure that the operator with smaller time argument is on the right hand side of the other one [66]. Hence, the Greens' function can be interpreted as an additional electron (or hole, depending on the time ordering) propagating from $t'$ to $t$ in a system described by the Hamiltonian $\hat{H}$ [66].

In this approach the calculation of photoelectron spectra is formulated such that the poles and residues of the Fourier transformed Greens' function are searched. This becomes clear when writing the time-ordering operator in equation (2.1) explicitly

$$G_{j,k}(t,t') = -\mathrm{i}\langle\Psi^N|\hat{a}_j(t)\hat{a}_k^\dagger(t')|\Psi^N\rangle\Theta(t-t') - \mathrm{i}\langle\Psi^N|\hat{a}_k^\dagger(t')\hat{a}_j(t)|\Psi^N\rangle\Theta(t'-t). \tag{2.2}$$

Inserting the closure relation $\hat{1} = \sum_k |\Psi_k^M\rangle\langle\Psi_k^M|$, where $M = N \pm 1$ and $|\Psi_k^M\rangle$ describes a bound state, between the operators in both terms of (2.2) the Lehmann representation [66] is obtained whose Fourier transform is

$$G_{j,k}(\omega) = -\mathrm{i}\sum_k \frac{\left|\langle\Psi^N|\hat{a}_j|\Psi_k^{N+1}\rangle\right|^3}{\omega - (E_k^{N+1} - E^N) + \mathrm{i}\nu} - \mathrm{i}\sum_k \frac{\left|\langle\Psi^N|\hat{a}_k^\dagger|\Psi_k^{N-1}\rangle\right|^2}{\omega + (E_k^{N-1} - E^N) - \mathrm{i}\nu}, \tag{2.3}$$

where $\nu$ is a small parameter arising from calculation of principal value. Further $\omega$ denotes the argument of the Fourier transform while $E^N$ and $E_k^M$ are the energies of the $N$-electron ground stated $|\Psi^N\rangle$ and of the $k$-th $M$-electron state $|\Psi_k^M\rangle$ respectively. In this form, the second sum corresponds to transitions in the photoelectron spectrum: the nodes of the denominator (poles of the Greens' function) can be easily assigned to the ionisation potentials and thus the transition energies in photoelectron spectra. Further, the integrals in the nominator are equivalent to the sudden approximation derived in chapter 2.3.3 and hence provide a good approximation to the transition strengths. The terms in the first sum correspond to the respective quantities of electron detachment [67].

However, computing the Greens' function is a demanding task which is of similar complexity as the computation of a solution to the SE. Over the years several approaches were developed of which the algebraic diagrammatic construction [67] and the equation of motion [60, 67] are the most prominent. In the diagrammatic construction one starts with an initial zeroth order Greens' function $\mathbb{G}^0(\omega)$ constructed in a Hartree-Fock basis and corrects it iteratively by $\mathbb{G}^0(\omega)\mathbb{\Sigma}(\omega)\mathbb{G}(\omega)$, where $\mathbb{\Sigma}(\omega)$ is the self-energy, an effective potential that is used to recover electron correlation and relaxation effects [68]. The self-energy usually is expanded in a perturbation series with respect to Feynman diagrams with increasing number of vertices and is exact in the limit of infinite terms [66, 69]. The one-particle energies, Coulomb matrix elements and overlap integrals are obtained from self-consistent field (SCF) calculations [67] which are usually obtained on the HF-level [68] but (TD)DFT or any other quantum chemical method can be used as well [18]. While being much easier to compute, the Hartree-Fock basis has the disadvantage that only single configurational electronic states can be treated.

On the other hand, an important advantage of the Greens' function method is that the transition energies are computed directly while in most other methods calculated it as the difference of the initial and final state functions. The latter approach however can lead to errors in the electron volt range when the interaction energies are badly estimated [67].

## 2.2 Combined Bound and Continuum State Representation

In contrast to the Greens' function method in which the explicit description of the FEF omitted, a large group of methods describes the full $N$-electron system before and after the ionisation respectively. With this approach electron correlation effects also between bound and unbound states are accounted for but a large and flexible basis is required which can represent bound as well as unbound states of electrons. Due to this, these methods are generally restricted to small systems that fulfil certain symmetry-requirements and have only a low amount of electrons.

The most prominent representative of this class in frequency-domain is the R-matrix method [70–72]. Its general idea is to conduct a partition of space into regions which are treated differently, connected by explicit boundary conditions to ensure smoothness of the wave function. These regions are constructed with concentric spheres, restricting the symmetry of wave functions in this scheme. Nonetheless it is applied not only to atoms [73–75] but also to small molecules [76, 77]. In the R-matrix formalism the inner region is chosen large enough to contain the bound part of the $N$-electron function that is usually represented by a configuration interaction (CI) expansion of Slater determinants (SDs), using a with a linear combination of atomic orbitals (LCAO) basis or a grid representation [72]. The FEF commonly is described by a linear combination of bound orbital type functions and continuum functions such as Coulomb waves [70, 71]. In the outer region, an expansion in Coulomb waves is used to ensure the asymptotically correct behaviour. In addition to the inner region, where correlation plays an important role, and the asymptotic outer region further intermediate regions can be added where the FEF is represented by a multipole-radiation expansion which is a polynomial of inverse powers of the distance to the centre [72].

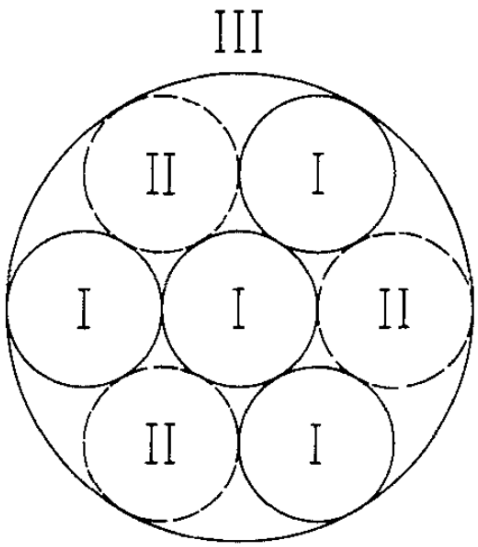


Figure 2.2: Schematic view of the space partition scheme used by Johnson for a four-atomic molecule: I: atomic, II: interatomic and III: extra-molecular space [78].

A generalisation to non-spherical systems is employed, *e.g.*, by Johnson [78] who used different kinds of non-concentric spheres. One set of spheres is centred each at an atom while others are placed such in the interatomic regions such that the space is filled as dense as possible as shown in Figure 2.2 for a molecule with four atoms. Each atom is located in the centre of a circle denoted as I while the circles II fill the interatomic space. An outer sphere surrounds the molecule to account for the asymptotic region similar to that used in R-matrix theory. In this scheme the exchange-correlation is treated on an approximate level [79] and is spherically averaged, resulting in a description that is equivalent to the muffin-tin potential which is a well-known model in solid state physics [80, 81]. The

continuity of the wave-functions as well as their derivatives is a ensured over the regions using multiple-scattered-wave theory [78]. The wave-functions are chosen in each region as a one-centre expansion of the form

$$\Psi(\boldsymbol{r}) = \sum_{l=2}^{l_{\max}} \sum_{m=-l}^{l} c_{l,m} R_l(r) Y_l^m(\theta, \phi) \tag{2.4}$$

where $r, \theta, \phi$ are the coordinates of the spherical coordinate system and $Y_l^m(\theta, \phi)$ are the spherical Harmonics [32]. The radial function $R_l(r)$ solves the radial SE

$$\frac{\partial^2 R(r)}{\partial r^2} + \left( E - V(r) + \frac{l(l+1)}{r^2} \right) R(r) = 0 \tag{2.5}$$

with the respective spherically averaged potential $V(r)$ [78].

An approach applied by DeCleva *et al.* to $H_2^+$ [25] and benzene [82] resigns the use of spheres, allowing for more general boundaries between the inner and outer regions. Here the FEFs are globally described in the one-centre expansion (2.4) where $R(r)$ is described by a B-spline basis. The advantage of the spline-based description is that smoothness at the interface of the regions is ensured intrinsically.

Another scheme in frequency domain is used by Richards and Larkins [83] with a hybrid ansatz: While the bound states of the $H_2$ molecule are described in the common LCAO scheme, the FEF is described by the product ansatz $\Psi(\boldsymbol{r}) = R(r, \theta) e^{im\phi}$ where $R(r, \theta)$ is obtained on a two-dimensional grid using a finite difference (FD) scheme. In contrast to the previously described methods, here no partition of space is conducted but instead a finite box with Dirichlet boundary conditions is used. Moreover, the FEF is treated on the HF-level, neglecting correlation effects [83].

Similar descriptions are used in time-domain by several authors [84–86]. Since a time-domain description requires the recomputation of the $N$-electron function for each time-step and thus several hundreds to thousands of times per simulation, its computational effort is increased by far. On the other hand, time-domain methods allow the description of non-linear effects such as high harmonic generation and multi-photon ionisation [10] which are both not perceptible by frequency-domain methods.

An important difference between time- and frequency-domain methods of practical means is that in time-domain free particles are described by a wave packet and hence as a localised function. Moreover, at short times after ionisation the continuum states often can be assumed to be coupled diabatically to the bound states (*i.e.* the wave packet does not move away from the ionic remainder). Under this assumption, the spacial part of the FEF can be written as a linear combination of bound state functions but having a complex energy that determines the oscillations and finite lifetime of the function [84]. Moreover a complex absorbing potential (CAP) (discussed in chapter 4.4.1 in more detail) is most often applied, ensuring the assumption of diabatic coupling to the bound states by cutting off that part of the wave function which is not localised at the molecule anymore. Due to these considerations the LCAO basis can be used here for the description of the free particles as well, as conducted *e.g.* by Jagau *et al.* [84]. In other simulations, grid-based descriptions are chosen using symmetry-adapted coordinate systems [86–89], allowing a product ansatz and hence a reduction in dimensionality. On the remaining one-dimensional grids often a

discrete variable representation (DVR) (described in section 3.3 of this thesis) is chosen. As an example, Yip *et al.* [90] simulate double ionisation of atomic beryllium in spherical coordinates, using the expansion (2.4) where $R(r)$ is separated into two regions in which a DVR and a finite element DVR (FE-DVR) scheme are used respectively. Tao *et al.* [86] as well as Bauch *et al.* [85, 91] use the FE-DVR basis in spheroidal coordinates respectively.

This is by far not a complete list; are these at least the most important methods?

## 2.3 The Dyson Orbital Formalism

The Dyson orbital (DO) formalism can be considered as an approximation to the formalisms described above where the free and bound states are described separately. Using such a separation leads to an neglect of correlation effects between the outgoing electron and the bound states and is often denoted as sudden ionisation limit [31, 33]. In this formalism the overlap between the initial state and the bound part of the final state is formulated as an effective one-electron quantity, called DO. Usually the DO scheme is considered in the frequency domain, but a time domain formulation exists as well and is described in the following subsection [92].

### 2.3.1 Time-dependent Dyson Orbitals

A good starting point for the DO formalism is an expansion of the time-dependent $N$-electron function $\Psi^N(\boldsymbol{r}, \boldsymbol{r}_2, \ldots, \boldsymbol{r}_N, t)$ in the form

$$|\Psi^N(t)\rangle = \frac{1}{\sqrt{N}} \sum_k |\Psi_k^{DO}(t)\rangle |\Psi_k^{N-1}\rangle e^{iE_k^{N-1}t} \tag{2.6}$$

where $E_k^{N-1}$ are the energies of the $N-1$-electron bound states described by the wave functions $|\Psi_k^{N-1}\rangle$ that are complete in the space of $N-1$-electron wave-functions. The expansion coefficients $|\Psi_k^{DO}(t)\rangle$ have the dimensionality of a one-particle function and are denoted as the time-dependent DO (TDDO). An important feature of the expansion (2.6) is that the dynamics of the $N$-electron system are reduced to a system of one-electron quantities $|\Psi_k^{\mathrm{DO}}(t)\rangle$ propagated by a TDDFT-like equation of motion [92]. Put the EOM here? In this approach the interaction of the DO with the bound states is approximated by the mean-field electrostatic potential [92], neglecting exchange and correlation.

The physical interpretation of the DO becomes clear when regarding its definition, given by

$$|\Psi_k^{\mathrm{DO}}(t)\rangle = e^{\mathrm{i}E_k^{N-1}t}\sqrt{N}\langle\Psi_k^{N-1}|\Psi^N(t)\rangle. \tag{2.7}$$

The remaining coordinates not integrated in (2.7) belong to the photoelectron since $|\Psi^{N-1}(t)\rangle$ is restricted to the description of bound states Hence in a frozen orbital approximation the DO is identical to the photoelectron. However, relaxation-effects change the overlap and thus lead to additional contributions to the TDDO. These considerations suggest to interpret the TDDO as a quasi-particle describing the electron that is ionised, including relaxation and correlation effects [33, 92].

### 2.3.2 Time-independent Dyson Orbitals

Working in frequency domain, no propagation of the TDDO nor the ionised system (2.6) needs to be considered. The time-independent DO is defined rather as the TDDO at $t = 0$. Since at this point the FEF is coupled adiabatically to the respective orbitals, the DO can be interpreted as quasi-particle that is ejected by the irradiating light [33].

The main advantage of this formalism in frequency-domain becomes clear when the photoelectron cross-section is considered. In the Fermis' Golden Rule formulation, which assumes the wavelength to be much larger than the system under study and weak irradiating light-field, the cross-section is in atomic units [31, 83]

$$\sigma(\epsilon) = \frac{2}{3}\nu \sum_k \left| \langle \Psi_i^N | \hat{\boldsymbol{d}} | \Psi_k^N \rangle \right|^2 \propto \sum_k |\boldsymbol{D}_k|^2 \tag{2.8}$$

where $\epsilon = \nu - (E_k - E_i)$ is the kinetic energy of the photoelectron that is determined by the photon energy $\nu$ and the energies $E_i$ of the initial unionised state $|\Psi_i^N\rangle$ and the total binding energy $E_k$ of the final ionised state $|\Psi_k^N\rangle$ which includes all electrons. Writing the initial and final states each as SDs

$$|\Psi_i^N\rangle = \hat{A}_N |\Phi_{i,1} \dots \Phi_{i,N}\rangle \tag{2.9a}$$

$$|\Psi_k^N\rangle = \hat{A}_N |\Phi_{k,1} \dots \Phi_{k,N-1} \Psi_k^{\mathrm{el}}\rangle \tag{2.9b}$$

where $\hat{A}_N$ is an $N$-electron antisymmetrisation operator. Furthermore the one-electron quantities $|\Phi_{k,j}\rangle$ denote the $j$-th (Kohn-Sham) orbitals and $\Psi_k^{\mathrm{el}}$ is the FEF. The index $k$ enumerates the final states which can have an arbitrary electron configuration here. The dipole operator $\hat{\boldsymbol{d}}$ is a one-electron operator that can be written as$\hat{\boldsymbol{d}} = \sum_{j=1}^N \hat{\boldsymbol{d}}_j$ where $\hat{\boldsymbol{d}}_j = \boldsymbol{r}_j$ in length gauge or $\hat{\boldsymbol{d}}_j = \nabla_j/(2\pi\nu)^2$ in velocity gauge respectively [83].

Using the SD representations (2.9), the integral $\boldsymbol{D}_k$ in equation (2.8) can be written as

$$\boldsymbol{D}_k = \langle \Phi_{i,1} \dots \Phi_{i,N} | \hat{A}_N \sum_{j=1}^N \hat{\boldsymbol{d}}_j \hat{A}_N | \Phi_{k,1} \dots \Phi_{k,N-1} \Psi_{\mathrm{el}} \rangle \tag{2.10}$$

where hermiticity of the antisymmetrisation operator is used. The expression (2.10) can be further expanded by commuting $\hat{A}_N$ with the dipole operator and making use of the relation $\hat{A}_N \hat{A}_N = \sqrt{N!}\hat{A}_N = \sum_P (-1)^p \hat{P}$ where the sum goes over all permutations $\hat{P}$ with parity $p$

$$\boldsymbol{D}_k = \sqrt{N!} \sum_P (-1)^p \sum_{j=1}^N \langle \Phi_{i,P(1)} \dots \Phi_{i,P(N)} | \hat{\boldsymbol{d}}_j | \Phi_{k,1} \dots \Phi_{k,N-1} \Psi_{\mathrm{el}} \rangle \tag{2.11}$$

$$= \sqrt{N!} \sum_P (-1)^p \sum_{j=1}^N \langle \Phi_{i,P(j)} | \hat{\boldsymbol{d}}_j | \Phi_{k,j} \rangle \langle \Phi_{i,P(1)} | \Phi_{k,1} \rangle \dots \langle \Phi_{i,P(j-1)} | \Phi_{k,j-1} \rangle \tag{2.12}$$

$$\times \langle \Phi_{i,P(j+1)} | \Phi_{k,j+1} \rangle \langle \Phi_{i,P(N-1)} | \Phi_{k,N-1} \rangle \dots \langle \Phi_{i,P(N)} | \Psi_{\mathrm{el}} \rangle \tag{2.13}$$

where $P(j)$ is a permutation of the $j$-th orbital. Thereby the term $j = N$ differs qualitatively from the others since the dipole operator acts on the FEF. Hence the sum can be

reordered to obtain

$$\boldsymbol{D}_k = \underbrace{\sqrt{N!}\sum_P (-1)^p \langle\Phi_{i,P(1)}|\Phi_{k,1}\rangle \dots \langle\Phi_{i,P(N-1)}|\Phi_{k,N-1}\rangle\langle\Phi_{i,P(N)}}_{\langle\Psi_k^{\mathrm{DO}}|} |\hat{\boldsymbol{d}}_j|\Psi_{\mathrm{el}}\rangle +$$
$$\sqrt{N!}\sum_P (-1)^p \sum_{j=1}^{N-1} \langle\Phi_{i,P(1)}|\Phi_{k,1}\rangle \dots \langle\Phi_{i,P(j-1)}|\Phi_{k,j-1}\rangle \times$$
$$\langle\Phi_{i,P(j+1)}|\Phi_{k,j+1}\rangle \dots \langle\Phi_{i,P(N-1)}|\Phi_{k,N-1}\rangle\langle\Phi_{i,P(j)}|\hat{\boldsymbol{d}}_j|\Phi_{k,j}\rangle\langle\Phi_{i,P(N)}|\Psi_k^{\mathrm{el}}\rangle \tag{2.14}$$

where the first sum is denoted as DO and the second as conjugate DO respectively [93]. To reduce the large amount of integrals therein, the strong orthogonality approximation is applied under the assumption that the overlap

$$\langle\Phi_{k,j}|\Psi_{\mathrm{el}}\rangle = 0 \quad \forall\, j = 1, \dots, N. \tag{2.15}$$

of the FEF with all bound states vanishes. This would be strictly valid if they would correspond to the same Hamiltonian. But in most cases the orbitals of the ionised and unionised state are similar, leading to small but non-zero overlaps [46, 93]. Applying the strong orthogonality condition leads to the drop out of the second sum in equation 2.14 and the transition dipole moment simplifies to

$$\begin{aligned}\boldsymbol{D}_k &= \sum_p (-1)^P \langle\Phi_{i,P(1)}|\Phi_{k,1}\rangle \dots \langle\Phi_{i,P(N-1)}|\Phi_{k,N-1}\rangle\langle\Phi_{i,P(N)}|\hat{\boldsymbol{d}}_j|\Psi_k^{\mathrm{el}}\rangle \\ &= \langle\Psi_k^{\mathrm{DO}}|\hat{\boldsymbol{d}}_j|\Psi_k^{\mathrm{el}}\rangle \end{aligned} \tag{2.16}$$

which corresponds to the definition of the TDDO in equation (2.7) for $t = 0$ as mentioned above. The expression for the PES cross-section in the DO formalism simplifies to

$$\sigma(\epsilon) = \frac{2}{3}(\epsilon + E_k - E_i) \sum_k \left|\langle\Psi_{\mathrm{DO}}^k|\hat{\boldsymbol{d}}|\Psi_{\mathrm{el}}\rangle\right|^2. \tag{2.17}$$

In the derivation given here, it is assumed that initial and final state can be represented by a single SD each. In practice, often states are described by a linear combination of SDs with different electron configurations. A respective generalisation of the DO is straight forward but introduces additional summations and thus leads to more complex terms.

### 2.3.3 Sudden Approximation

Further simplification of the DO formalism can be obtained by applying the so-called sudden approximation (SA) where the computation of the FEF is avoided. In the SA it is assumed that the transition to a continuum function with corresponding energy has a constant probability which can be justified by the high degree of degeneracy of continuum functions for each given energy. Thus, the transition probability

$$\boldsymbol{D}_k = \sum_p (-1)^P \langle\Phi_{i,P(1)}|\Phi_{k,1}\rangle \dots \langle\Phi_{i,P(N-1)}|\Phi_{k,N-1}\rangle\langle\Phi_{i,P(N)}|\hat{\boldsymbol{d}}_j|\Psi_{\mathrm{el}}\rangle \tag{2.18}$$

reduces to

$$D_k = \sum_p (-1)^P \langle \Phi_{i,P(1)} | \Phi_{k,1} \rangle \dots \langle \Phi_{i,P(N-1)} | \Phi_{k,N-1} \rangle \tag{2.19}$$

which is the probability for the bound $N-1$-electron system to conduct the transition between the respective bound states of the unionised and ionised system [94]. With this assumption the kinetic energy dependence of the PES is neglected, assuming error introduced is a similar factor for all transitions. This has shown to be a valid assumption if the nature and spacial extend of the Dyson orbitals is similar.

Moreover, the expression (2.19) corresponds to the nominator of the Greens' function in (2.3) and thus is the level of theory at which the Greens' function PES transitions are computed.

Finally, the expression (2.19) can be further simplified to get the approach described in the introduction of this chapter, based on Koopmans' theorem. Therefore the electron relaxation is neglected and thus the $N-1$-electron state can be written as $|\Psi_k^{N-1}\rangle = \hat{a}_k |\Psi_i^N\rangle$. Thus, the sum over all permutations $\hat{P}$ in (2.19) reduces to the case where $P(j) = j \, \forall j = 1, \dots, N-1$ due to orthogonality of the orbitals. Moreover, due to the normalisation of the orbital functions, all transitions have a probability of one and thus corresponds to the scheme described earlier.

# 3 | Description of Free Particles

The description of particles in continuum states bears several complications of conceptual and technical kinds. In this chapter different numerical methods are introduced that can be used to solve the one-electron SE. In section 3.1 the conceptual differences between bound and continuum states as well as the numerical treatment of the latter in a finite basis are discussed. Thereafter, in the sections 3.2 - 3.7 different numerical methods are introduced that can be used to solve the one-particle SE on a molecular domain.

## 3.1 Continuum Waves

Continuum waves are discussed only sparsely in lectures on quantum mechanics, even though they posses certain properties of fundamental difference compared to bound states. The states considered here have a spatially infinite extend as it is well-known for plane waves $\Psi(\boldsymbol{r}) = e^{i\boldsymbol{k}\boldsymbol{r}}$ as well as spherical waves. Morover, these waves are not square integrable and hence can not be normalised according to $\int \Psi^\dagger(\boldsymbol{r})\Psi(\boldsymbol{r})d\boldsymbol{r} = 1$ and so the probability interpretation is invalid [95]. Instead, these functions are sharp in a continuous variable (namely the momentum) and hence should rather be interpreted as probability densities, suggesting the normalisation $\int \Psi^\dagger(\boldsymbol{r})\Psi(\boldsymbol{r'})d\boldsymbol{r} = \delta(\boldsymbol{r}-\boldsymbol{r'})$ where $\delta(\boldsymbol{r})$ is the Dirac delta distribution [95]. This property distinguishes the analytical FEF from those obtained from numerical methods that often have a finite extend and are obtained from an approximate Hamiltonian which has no continuous spectrum due to finiteness of its basis. This difference in the dimensionality of the wave functions also affects the integral evaluated when calculating the transition dipole matrix elements [96]. Nonetheless this problem can be resolved by the Stieltjes-Imaging approach described in the subsection 3.1.1. The Stieltjes-imaging technique moreover can be used to varify the use of a square-integrable function for the representation of a continuum state since it can be considered as 0-th order moment expansion.

A second aspect that is only sparsely discussed in literature concerns the question of what the numerical solution corresponds to. When dealing with approximate continuum functions, it is often assumed that the analytical function of interest $|\Psi_\mathrm{a}(\boldsymbol{k})\rangle$ is approximated by that particular numerical solution $|\Psi_\mathrm{n}(\boldsymbol{k'})\rangle$ which is closest in energy [25]. An alternative interpretation would be to assume that the numerical solution corresponds to an approximation to $|\Psi_\mathrm{n}\rangle \approx \frac{1}{k^+-k^-}\int_{k^-}^{k^+}|\Psi(k)\rangle dk$ which would change the interpretation and normalisation of the respective numerical solution.

A further conceptual problem is due to degeneracy of the analytical solution. This issue becomes apparent when considering the ionisation of a hydrogen-like atom whose

analytical FEF is well-known and has the form

$$\Psi_{\boldsymbol{k}}(\boldsymbol{r}) = \frac{1}{(2\pi)^{\frac{3}{2}}} \frac{1}{r} \sum_{l=0}^{\infty} \sum_{m=-l}^{l} c_{l,m} w_l \left( \frac{Z}{r}, rk \right), Y_l^m(\theta, \phi)\, Y_l^m(\theta_k, \phi_k) \tag{3.1}$$

where $Z$ is the change of the nucleus, $k = |\boldsymbol{k}|$ is the absolute value of the wave vector $\boldsymbol{k}$ and the arguments to the spherical Harmonics $Y_l^m$, $(\theta, \phi)$ and $(\theta_k, \phi_k)$, are the angles of the spherical coordinate system in real-space and Fourier-space respectively [33]. Finally $w_l\left(\frac{Z}{k}, rk\right)$ is the radial wave function that can be expanded in an infinite term of confluent hypergeometric functions [32].

The function (3.1) is, given its energy $E = \frac{1}{2}|\boldsymbol{k}|$, degenerate in the direction of $\boldsymbol{k}$ as well as in the quantum numbers $l$ and $m$ with infinite terms respectively. Hence the wave function of a photoelectron can consist of any superposition of the form (3.1), chosing the coffecients $c_{l,m}$ accordingly. The coefficients $c_{l,m}$ of the physically observable FEF are determined by the overlap integrals with the DO (2.16). Considering as an example the ionisation of hydrogen in its ground state, the FEF will allways be in one of the three $p$-waves because the probability to access any of the other vaccum-states with the correct energy vanishes.

Unfortunately, the considerations made above are not true for the numerical solution anymore where a finite set of superpositions is obtaind which, due to numerical treatment, differ in energy and thus can not be assigned to a common value of $\boldsymbol{k}$. Chosing the energetically best-fitting solution though might result in a function with vanishing contribution of the $p$-type orbitals while, for slightly changed paraters or target energy (or even just using an other computer) could yield a solution with large contributions with $l = 1$.

### 3.1.1 Stieltjes Imaging

The Stieltjes imaging provides an elegant way to still use the numerially obtained solutions of a non-continuous spectrum by using moment theory. Starting from the expression for the photoelectron spectrum

$$\sigma(\varepsilon) \propto \left| \langle \Psi_0 | \hat{d} | \Psi_{\text{el}} \rangle \right|^2 \tag{3.2}$$

where $\Psi_{\text{el}}$ is a continuum function and as such, as discussed above, not square integrable which is an important characteristic for the dimensionality of this expression [96]. To repair this, in the Stieltjes imaging approach the $n$-th spectral moment

$$M_n = \langle \Psi_0 | \hat{d} (\hat{H} - E_0)^n \hat{d} | \Psi_0 \rangle \tag{3.3}$$

where $\hat{H}$ is the systems Hamiltonian and $E_0$ is the ground state energy [97]. Inserting the closure relation $\sum_\alpha |\Psi_\alpha\rangle\langle\Psi_\alpha| + \int |\Psi_\varepsilon\rangle\langle\Psi_\varepsilon| d\varepsilon$ for the full (anatlytic) Hamiltonian results in

$$M_n = \sum_\alpha \langle \Psi_0 | \hat{d} (\hat{H} - E_0)^n | \Psi_\alpha \rangle \langle \Psi_\alpha | \hat{d} | \Psi_0 \rangle + \int \langle \Psi_0 | \hat{d} (\hat{H} - E_0)^n | \Psi_\varepsilon \rangle \langle \Psi_\varepsilon | \hat{d} | \Psi_0 \rangle d\varepsilon \tag{3.4}$$

$$= \sum_\alpha E_\alpha^n \left| \langle \Psi_0 | \hat{d} | \Psi_\alpha \rangle \right|^2 + \int \varepsilon^n \left| \langle \Psi_0 | \hat{d} | \Psi_\varepsilon \rangle \right|^2 d\varepsilon. \tag{3.5}$$

However, inserting the unity expression for the numerical Hamiltonian which does not have continuum functions but an everywhere discrete spectrum and hence $L^2$-integrable eigenfunctions results in

$$M_n = \sum_j^N (E_j - E_0)^n \left| \langle \Psi_0 | \hat{d} | \Psi_j \rangle \right|^2 \tag{3.6}$$

to be evaluated [96] for the $N$ eigenfunctions $|\Psi_j\rangle$. For a good numerical approximation, the expressions (3.6) and (3.4) should be similar for as many $n$ as possible. These considerations are used in the Stieltjes imaging approach with moment theory [98, 99].

In the protocol derived from this scheme thus the oscillator strength $|\langle \Psi_0 | \hat{d} | \Psi_{\mathrm{el}} \rangle|^2$ is approximated by the histogram

$$\sigma(\varepsilon) = \frac{2}{3}\frac{df}{d\varepsilon} = \frac{2}{3} \begin{cases} 0 & 0 < \varepsilon < \varepsilon_1(n) \\ \frac{1}{2}\frac{(f_i + f_{i+1})}{\varepsilon_{i+1} - \varepsilon_i} & \varepsilon_j(n) < \varepsilon < \varepsilon_j + 1(n) \\ 0 & \varepsilon_n(n) < \varepsilon \end{cases} \tag{3.7}$$

where $f_i$ is obtained from enforcing the relation (3.6) for $n = 1, \ldots, N$ which is done by solving the matrix equation

$$\boldsymbol{M} = \mathbb{E}\boldsymbol{f} \tag{3.8}$$

where $\boldsymbol{f}_i = f_i$, $\boldsymbol{M}_i = M_i$ and $\mathbb{E}_{i,j} = \varepsilon_i^j$ [97]. It can be shown moreover that $M_n$ is only for $n < 2$ finite and therefore negative moments are used [96]. Moreover, it can be shown that the expression (3.6) converges already for small $N$, so only a small fraction of the spectrum needs to be considered in practice and the matrix equation (3.8) remains at a reasonable size.

In practice this method becomes very demanding if energetically narrow transitions occur since many terms in expression (3.6) are needed for convergence, making this method effective mainly for low energy range [25]. Another disadvantage that no asymtotic information about this scheme present [25].

## 3.2 Finite Differences and Finite Volumes

The most common and straightforward approach to solve differential equations numerically is via the so-called finite difference (FD) scheme. Starting from the one-particle SE in atomic units

$$\left( \frac{1}{2}\nabla^2 V(\boldsymbol{r}) \right) \Psi(\boldsymbol{r}) = E\Psi(\boldsymbol{r}) \tag{3.9}$$

where $V(\boldsymbol{r})$ is an arbitrary potential at this point. Considering a general problem where the low symmetry does not support a product ansatz which would reduce the dimensionality and thus the complexity of the problem, the kinetic energy operator has at least 6 non-diagonal terms which lead to an Hamiltonian of a non-banded structure [100]. Moreover, the finite-difference schemes require the evaluation points to be on a regular grid whose size is governed by the sharpest features in the system while local refinement is hardly available. To resemble the expected fine structure close to the nuclei, a dense grid is needed but any FD scheme beyond the first order requires the evaluation points to be on a

regular grid, making the computation of a FEF with a reasonable box size very expensive [83]. Nonetheless, there are applications to this scheme to the SE [100, 101], some of them with massive parallelisation using MPI and multiple GPUs [102].

To overcome this bottleneck for systems with non-uniform parameters, often the finite volume method is used. The finite volume method is an integral method that is not based on a regular grid. Instead, for the estimation of the kinetic energy Gauß's theorem $\int_V \nabla \boldsymbol{u}(\boldsymbol{r}) dV = \int_{\partial V} \boldsymbol{u}(\boldsymbol{r}) \boldsymbol{n} dS$ is used where $\boldsymbol{u}(\boldsymbol{r})$ is a vector-valued function and $\boldsymbol{n}$ is the normal vector on the surface $S$ of the volume $V$ under consideration. Chosing $\boldsymbol{u}(\boldsymbol{r}) = \nabla\Psi(\boldsymbol{r})$ yields the relation

$$\nabla^2\Psi(\boldsymbol{r}) = \lim_{V\to 0} \frac{\int_{\partial V} \nabla\Psi(\boldsymbol{r}) \boldsymbol{n} dS}{V}. \tag{3.10}$$

This scheme becomes especially interesting when the finite volume elements are chosen to be Voronoi cells [103]. A Voronoi-tesselation is associated with a grid and is constructed such that the Voronoi cell $T_i$ consists of all points in space that are closer to the point $i$ than to any other points in the grid [104–106].

This description has the advantage that the quantities on the right-hand side of (3.10) can be associated with properties of the Voronoi-Cell, leading to the first-order approximation of the kinetic energy

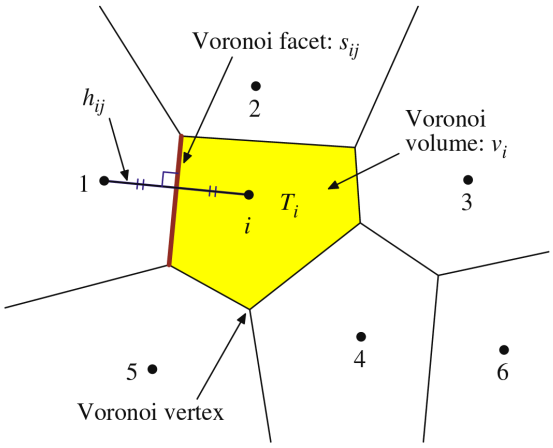


Figure 3.1: 2-dimensional Voronoi diagram on an arbitrary point-distribution. [107]

$$\nabla^2\Phi(\boldsymbol{r}_i) = \frac{1}{v_i} \sum_j^{\text{neighbours}} \frac{\Psi(\boldsymbol{r}_j) - \Psi(\boldsymbol{r}_i)}{h_{ij}} s_{ij} a \tag{3.11}$$

where $v_i$ is the volume of the $i$-th Voronoi-cell, $h_{ij} = |\boldsymbol{r}_i - \boldsymbol{r}_j|$ is the distance between the centres of the $i$-th and $j$-th Voronoi-cell and $s_{ij}$ is the lengthe of the common facet of the $i$-th and $j$-th Voronoi cell.

Such a scheme is applied *e.g.* by Son and Chu [103, 107] to the time-dependent SE, studying multi-photon ionisation of several molecular systems.

## 3.3 Pseudospectral Methods

Under the term (pse)udospectral methods a large group of methods is comprised which treat the differential equation of interest variationally using an orthogonal basis $span\{\varphi_i(\boldsymbol{r})\}$, hence seeking for a solution of the form

$$\Psi(\boldsymbol{r}) = \sum_i^n c_i \varphi_i(\boldsymbol{r}) \tag{3.12}$$

where $c_i$ are coefficients to be found [108]. In the pseudospectral methods the ansatz functions $\varphi_i(\boldsymbol{r})$ thereby are smooth global functions such as $\varphi_{\boldsymbol{k}}(\boldsymbol{r}) = \frac{1}{(2\pi)^{\frac{3}{2}}} e^{\mathrm{i}\boldsymbol{k}\boldsymbol{r}}$ resulting in the Fourier method [109]. Alternatively Jacobi, Chebychef or Legendre polynomials are commonly used [110].

To find the corresponding coefficients, the equation is evaluated on a grid, leading to a linear system of equations to be solved. Depending on the technique used for determining the coefficients, it can be seen as a high-order FD or high-order ($p$-) finite element method (FEM). One large advantage of this class of methods is that the error of the solution $\psi(\boldsymbol{r})$ usually decays exponentially with the number $n$ of ansatz functions and the grid can be chosen coarsely, making the numerical scheme very efficient [110, 111]. In addition, many formulations allow for an implementation making use of the fast fourier transform [110].

A special representative subgroup of the pseudospectral methods are the so-called discrete variable representation (DVR) schemes which are frequencly used to study quantum chemical problems [90, 112, 113]. Since this scheme is applicable in one dimension only, often symmetry-adapted coordinates such as spherical coordinates are used and the ansatz

$$\varphi = \sum_{l,m} R_{l,m}(r) Y_l^m(\theta, \phi) \tag{3.13}$$

is applied where $Y_l^m(\theta, \phi)$ are the well-known spherical harmonics [114] and $R_{l,m}(r)$ are radial functions that are computed explicitly, solving the radial SE.

The ansatz functions used therein usually are Lagrange polynomials [86, 112, 113] whose nodes are chosen by a general Gaußquadrature rule [112] or from a quadrature rule for the radial Coulomb function which is in particular popular for quntum chemical problems [111, 113]. Even if the DVR provides a flexible and fast-convergent basis, an extension to higher dimensionality can be achieved by a product ansatz only and thus is applicable to problems with high symmetry only.

Moreover, as for the other pseudospectral methods, the system matrices are dense and thus the solution is numerically expensive. This is, at least in parts, solved by using a hybrid scheme of the finite element and DVR scheme where the DVR scheme is used on small segment only, connected by single bridge-functions each [86, 112].

## 3.4 Radial Basis Functions

The radial basis function (RBF) technique is a basis that is based on an arbitrary point distribution with very general properties. The basis functions $\varphi_i(\boldsymbol{r})$ used in this technique need to be spherically symmetric, *i.e.* $\varphi_i(\boldsymbol{r}) = \varphi_i(|\boldsymbol{r}|)$ and are placed at the grid points of a given domain. Among the commonly used functions are, besides linear and cubic functions, multiquadratic ($\sqrt{r^2 + r0^2}$), inverse multiquadratic ($\frac{1}{\sqrt{r^2+r0^2}}$) and Gaussian ($e^{-\frac{r^2}{2r_0^2}}$) functions [115, 116].

If the parameter $r_0$ is chosen reasonably the scheme is numerically stable and fast-convergeing [115]. Another advantage is the straight-forward implementation and generality of this method. But the coise of $r_0$ can be non-trivial especially for highly non-regular grids where the occurring large distances require broad and smooth functions which lead

to instabilities for close-lying points. Moreover the resulting system matrices are dense due to the global definition of the ansatz functions, making it compputationally expensive.

The RBF-scheme is used not only for solving differential equations but is also a usefull tool for interpolation of scattered data in arbitrary dimensions [117] and surface reconstruction from scattered data [118].

An important disadvantage of the RBF scheme is that the space between two interpolation points is interpolated non-linearly and, depending on the distance of the two functions, the values are over- or underestimated. This error is visualised in Figure 3.2 for the case of a function that is one at both supporting points, represented by a Gaussian RBF basis. The intermediate course of the function depends strongly on the ratio of the broadening $r_0$ and the difference between the supporting points.

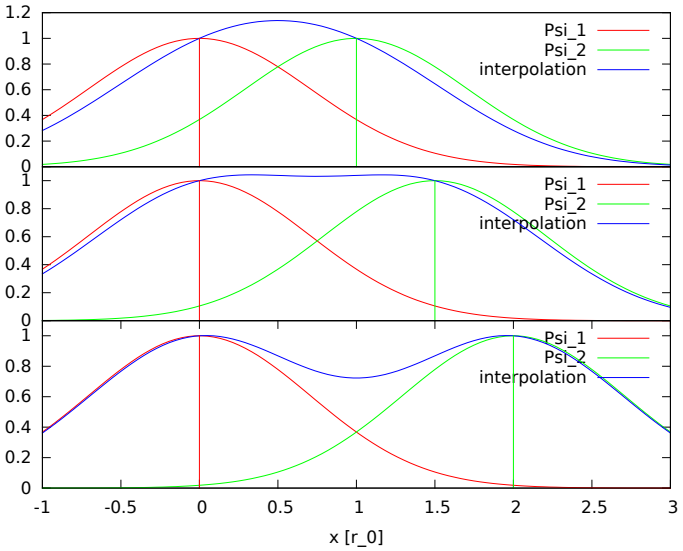


Figure 3.2: A function (blue) represented in a RBF basis with Gaussian functions, centred at different distances compared to the broadening parameter $r_0$.

While this behaviour is not problematic for visual purposes, it may introduce a substructure which can lead to unintended behaviour of the solution. Since on irregular grids strongly varying distances between supporting points occur, this behaviour is stronger the less regular the initial data are.

## 3.5 Finite Elements

In the FEM the differential equations to be solved are formulated in their weak form that can be understood as a generalisation of it. Starting with the well-known (strong) form of the SE defined on a domain $\Gamma$ in atomic units which are used here and in the following chapters

$$-\frac{1}{2}\nabla^2\Psi(\boldsymbol{r}) + V(\boldsymbol{r})\Psi(\boldsymbol{r}) = E\Psi(\boldsymbol{r}) \qquad \boldsymbol{r} \in \Gamma \tag{3.14}$$

with the condition for the boundary domain $\partial\Gamma$ which is assumed to be Lipschitz continuous

$$\Psi(\boldsymbol{r}) = 0 \qquad \boldsymbol{r} \in \partial\Gamma. \tag{3.15}$$

Thereby the first term in equation (3.14) corresponds to the kinetic energy and $V(\boldsymbol{r})$ is a potential that is not further specified at this point. The unknowns of this equation are the wave function $\Psi(\boldsymbol{r})$ and respective energy $E$. To bring equation (3.14) into the weak form, it is first multiplied by a test function $\Phi(\boldsymbol{r})$ which fulfils the same boundary conditions and needs to be differentiable. In the second step, one integrates over the whole space of

interest resulting in

$$\int d\boldsymbol{r}\left(-\frac{1}{2}\left(\nabla^2\Phi(\boldsymbol{r})\right)\Psi(\boldsymbol{r})+V(r)\Phi(\boldsymbol{r})\Psi(\boldsymbol{r})\right)=E\int d\boldsymbol{r}\Phi(\boldsymbol{r})\Psi(\boldsymbol{r}). \tag{3.16}$$

Thereby the kinetic energy term can be symmetrised using Green's first identity $\int_\Gamma(\nabla^2\Psi)\Phi d\boldsymbol{r} = \int_{\partial\Gamma}(\nabla\Psi)\Phi ds - \int_\Gamma(\nabla\Psi)(\nabla\Phi)$ to obtain the final expression

$$\int d\boldsymbol{r}\left(\frac{1}{2}\left(\nabla\Phi(\boldsymbol{r})\right)\left(\nabla\Psi(\boldsymbol{r})\right)+V(r)\Phi(\boldsymbol{r})\Psi(\boldsymbol{r})\right)=E\int d\boldsymbol{r}\Phi(\boldsymbol{r})\Psi(\boldsymbol{r}) \tag{3.17}$$

$$\Phi(\boldsymbol{r})=0 \quad \Psi(\boldsymbol{r})=0 \quad \boldsymbol{r}\in\Gamma \tag{3.18}$$

which is denoted as the weak form of the SE. A function $\Psi(\boldsymbol{r})$ is considered as a solution of (3.17) if the equation holds for any test function $\Phi(\boldsymbol{r})$. Thereby for any function solving (3.14) the equation (3.17) is still valid but the space of solutions of the weak form is larger since only first derivatives need to be defined. In addition, a solution of (3.17) is defined only up to a cardinal number of zero; hence changing the values of a given solution $\Psi(\boldsymbol{r})$ along a finite number of planes in three dimensions yields a function that still solves (3.17). These properties play an important role here since they allow *e.g.* for piecewise linear ansatz functions as they are commonly used in the FEM scheme which do not have a second derivative and whose first derivative is undefined on areas with a cardinal number of zero.

To obtain the finite element formulation, one does not work on the whole space of differentiable and quadratically integrable functions defined on $\Gamma$ but restricts the space to subspace spanned by a finite set of test functions for both $\Psi(\boldsymbol{r})$ and $\Phi(\boldsymbol{r})$, leading to the Petrov-Galerkin scheme. To get best flexibility for the wave function, the domain $\Gamma$ is subdivided into finite volume elements with a close packing. These volume elements, denoted as finite elements, give this method its name. Having this subdivision of space, the ansatz (basis) functions $\varphi(\boldsymbol{r})$ used to construct $\Psi(\boldsymbol{r})$ and $\Phi(\boldsymbol{r})$ are defined as piecewise polynomials being non-zero only on one or few elements.
Considering $\Gamma$ to describe a plane, the elements can be for example triangles as shown in Figure 3.3. In this plane the vertices of the triangles can be enumerated as $\boldsymbol{r}_i\, i = 1,\ldots,N$, leading to the definition of piecewise linear ansatz functions

$$\varphi_i(\boldsymbol{r}_j)=\begin{cases}1 & j=i\\ 0 & j\neq i\end{cases} \tag{3.19}$$

resulting it two dimensional "hat" functions as depicted in Figure 3.3. The so defined basis ensures continuity of the solution over $\Gamma$ while the first derivatives are continuous only within each element. To assure continuity of

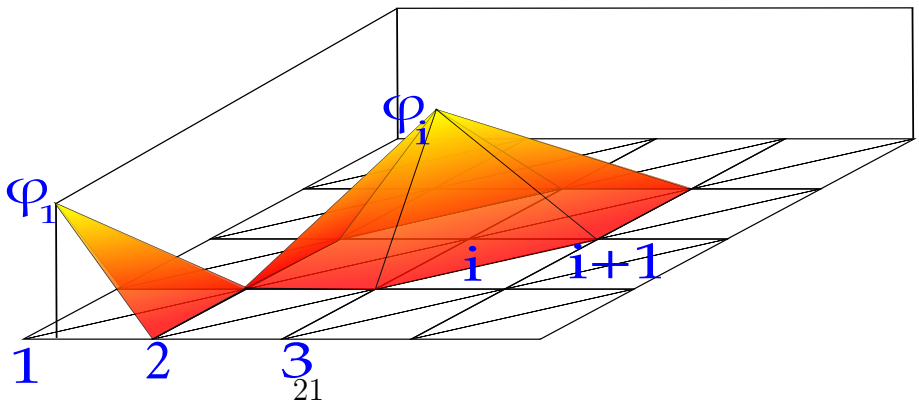


Figure 3.3: Example of finite elements in 2D of triangular shape and linear ansatz functions $\varphi_i(\boldsymbol{r})$ defined on them.

the first derivatives as well, second order polynomials are needed.

As usual in variational schemes, the wave function of interest is a linear combination of these basis functions $\Psi(\boldsymbol{r}) = \sum_i c_i \varphi_i(\boldsymbol{r})$ where $c_i$ are weighting coefficients. The test functions are chosen from the same space of ansatz functions, testing each basis separately $\Phi(\boldsymbol{r}) = \varphi_j(\boldsymbol{r}), j \in 1, \ldots, N$. Hence, the SE (3.17) is rewritten as

$$\sum_i \int d\boldsymbol{r} \left( \frac{1}{2} \left(\nabla \varphi_i(\boldsymbol{r})\right) \left(\nabla \varphi_j(\boldsymbol{r})\right) + V(r) \varphi_i(\boldsymbol{r}) \varphi_j(\boldsymbol{r}) \right) c_i = E \sum_i \int d\boldsymbol{r} \varphi_i(\boldsymbol{r}) \varphi_j(\boldsymbol{r}) c_i \quad \forall j \in \{1, \ldots, N\} \tag{3.20}$$

which is the $j$-th component of the generalised matrix eigenvalue problem

$$\left( \frac{1}{2} \mathbb{A} + \mathbb{V} \right) \boldsymbol{c} = E \mathbb{M} \boldsymbol{c}. \tag{3.21}$$

with

$$\mathbb{A}_{ij} = \int d\boldsymbol{r} \left(\nabla \varphi_i(\boldsymbol{r})\right) \left(\nabla \varphi_j(\boldsymbol{r})\right) \quad \mathbb{V}_{i,j} = \int d\boldsymbol{r} V(r) \varphi_i(\boldsymbol{r}) \varphi_j(\boldsymbol{r}) \quad \mathbb{M}_{i,j} = \int d\boldsymbol{r} \varphi_i(\boldsymbol{r}) \varphi_j(\boldsymbol{r}) \tag{3.22}$$

and the vector $\boldsymbol{c}$ in equation (3.21) contains the coefficients $c_i$ to be found.

The quality of this basis depends strongly on the size and shape of the finite elements: The stronger the solution varies, the smaller be should the elements, or it should have higher order ansatz functions to be able to represent the wave function. Knowledge about ranges of sharp structures and areas with smooth variation of the wave function $\Psi(\boldsymbol{r})$ hence is crucial for the setup of a good mesh.

In the next chapter more details about the finite element formulation will be given with a special focus on how to setup a grid that is well suited for describing free particles in quantum mechanics.

## 3.6 Hybrid Methods

In addition to the three methods presented above also mixed forms of these exists, utilizing the advantages of the respective ideas. One of the most prominent combinations of the above-mentioned methods is the finite element discrete-variable representation (FE-DVR) [86, 112]. Therein a DVR scheme is used with a set of ansatz functions each defined on a given interval only, the finite element. A single function connects these intervals respectively, similarly to the hat functions in FEM. Using this approach, more flexibility is obtained by varying the size of the elements or the number of basis functions per element.

Moreover, the usually dense matrix of DVR schemes changes to a block-structure, each coupled by only one row [86].

Another scheme resulting in a similar description to the above-mentioned which is used by several authors on quantum mechanical problems is the spectral element method [119]. In contrast to the FE-DVR-scheme it is based on the weak formulation and uses Chebychev or Lagrange polynomials and hence allows for larger elements than usual FEM. While the spectral elements are found to be well suited for linear problems they require a complex implementation and lead to denser system matrices. The larger density in general leads to a reduced numerical stability and is computationally more expensive. Finally, complex geometries usually benefit more from smaller elements that from higher orders [120].

A successfull variety of spectral elements and the finite element method is the so-called spectral difference method. Thereby a spatially uniform grid is used (as usual in the finite difference scheme) while employing a stepwise defined pseudospectral basis. The appealing properties of this method are an exponential convergence as known from finite difference methods by employing the sparsity of the equation system obtained in FEM [121].

More advanced methods based on the above-mentioned schemes are available as well [122, 123] but are not described in more detail for brevity.

## 3.7 Wavelets

The wavelet method was developed only in the 1980s [124] and combines the advantages of the Fourier method and FEM by decomposing objects into features of different scales and being a local method at the same time [124–126]. Even though it posesses very advantagous features, it is not very well-known untill today and not widely used in most subjects of science. The most prominent and widely distributed application of Wavelets is compression of data as used for example in the jpeg2000 standard [127].

A wavelet thereby denotes a basis of the function space $L_p(\mathbb{R}^d)$ *i.e.* the space of functions $\phi(\boldsymbol{r})$ for which $\int \phi(\boldsymbol{r})^p d\boldsymbol{r} < \infty$. The wavelet basis is defined via a finite set of orthonormal functions $\varphi_i(\boldsymbol{r})$, denoted as mother wavelets, by

$$\varphi_{i,j,\boldsymbol{\alpha}}(\boldsymbol{r}) = m^{\frac{j}{2}} \varphi_i(\mathbb{M}^j \boldsymbol{r} - \boldsymbol{\alpha}) \tag{3.23}$$

where $\mathbb{M}$ is an expanding scaling matrix (*i.e.* all eigen values have modulus larger than one), $m = |det(\mathbb{M})|$ and $j \in \mathbb{Z}\, \boldsymbol{\alpha} \in \mathbb{Z}^d$ are running indices. The condition for (**??**) to be a wavelet basis is that these functionst span $L_p(\mathbb{R}^d)$ [125]. In practice, this very general definition is often restricted by additional requirements such as orthogonality of $\varphi_{i,j,\boldsymbol{\alpha}}(\boldsymbol{r})$ with respect to $j$ and $\boldsymbol{\alpha}$. For brevity, in the following only the space $L_2(\mathbb{R})$ with $\mathbb{M} = 2$ is considered which corresponds to the initial definition of the wavelet basis [128]. The most prominent and by far simplest example of a wavelet is the so-called Haar-wavelet wich hase one mother waveletof the form

$$\varphi(x) = \begin{cases} 1 & 0 \leq x < \frac{1}{2} \\ -1 & \frac{1}{2} \leq x < 1 \\ 0 & \text{else} \end{cases} \tag{3.24}$$

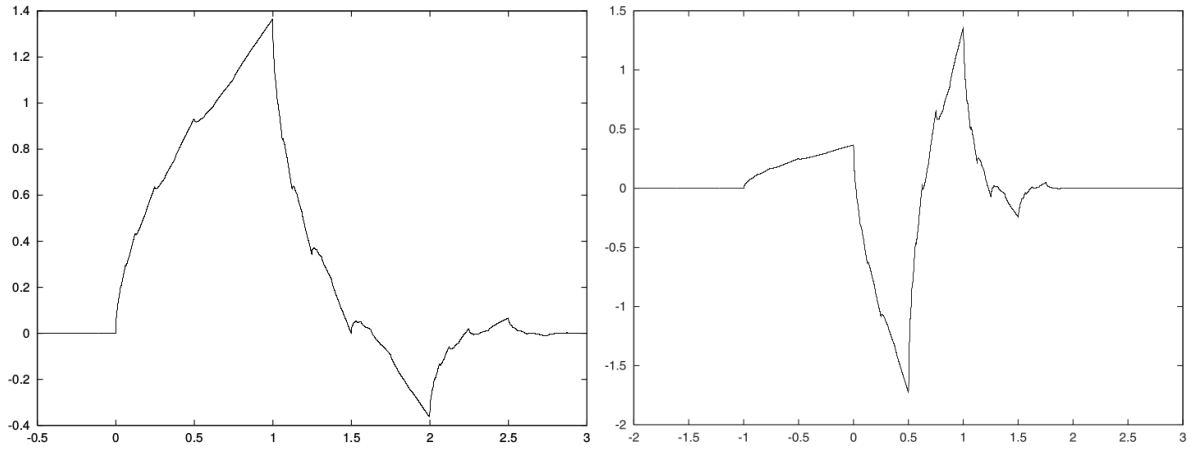


Figure 3.4: Dauberchies wavelet (b) and the respective scaling function (a).

for which (**??**) is a orthonormal basis with a compact support. In practice wavelets often are constructed via a scaling function $\chi(\boldsymbol{r})$ which need to fulfill the two-scale relation

$$\chi(x) = \sum_{k\in\mathbb{Z}} h_{1-k}\chi(2x-k) \tag{3.25}$$

with $||\chi||_{L_2} = 1$, leading to a unique definition via the coefficients $h_{1-k}$. From scaling function a wavelet is defined as

$$\varphi(x) = \sum_{k} (-1)^{k+1} h_{1-k}\chi(2x-k) \tag{3.26}$$

which is denoted as the look the name up relation. The above-mentioned Haar-wavelet than is defined by the coefficients $h_0 = 1$ and $h_1 = -1$. Another orthogonal wavelet with compact support is the Dauberchies-wavelet defined by the coefficients $h_0 = h_1 = \frac{1+\sqrt{3}}{4}$ and $h_2 = h_3 = \frac{1-\sqrt{3}}{4}$ which results in a mother-wavelet of the form

$$\varphi(x) = \frac{1+\sqrt{3}}{4}\chi(2x-1) - \frac{1+\sqrt{3}}{4}\chi(2x) + \frac{1-\sqrt{3}}{4}\chi(2x+1) - \frac{1-\sqrt{3}}{4}\chi(2x+2) \tag{3.27}$$

which already cannot be written in a closed form. Both wavelets mentioned above are not smooth functions but still posess good properties for practical applications. Further it is important to note that the explicit evaluation of the functions is not needed for most applications but one rather handles with the coefficients $h_k$ instead. More smooth wavelet can be obtained at the expense of a non-compact support but they usually decay fast and hence still can be considered as being localised.

Besides their broad use in data compression and analysis, they provide a good basis to solve partial differential equations and are found to have similar numerical properties to FEM sources[126].

# 4 | Finite Element Methods

As a conclusion of the previous chapter one can see that the number of methods that are currently available to describe a free electron function in presence of an intricate electrostatic background potential is not that large. In this work the method of choise to model the free electron function is the FEM which had been applied to quantum mechanical problems already by several authors [129–132], however, to the best of my knowledge, only to bound state problems so far. A brief review about these works is given in section 4.1. Besides its large flexibility and computational efficiency pointed out in section 3.5 already, the large amount of available libraries for FEM [54, 133–136] is another advantage of practical importance due to the complexity of the generation of a suitable mesh, assembling of matrices and solution of matrix equations.

In the following chapter the integration of the matrix elements (section 4.2) and set up of the mesh (section 4.3) will be described. Thereby the focus is put on the application to the one-particle SE that is to be solved with molecular electrostatic potential. Since the interest thereby is on free particle solutions, the spectrum is expected to be very dense and the wave function to be delocalised, requirering for well-designed boundary conditions. A discussion of various boundary conditions and asymptotic descriptions available for FEM is described in section 4.4.

## 4.1 Finite Element Calculations in Quantum Chemistry

The FEM is mainly known from engineering disciplines where it is used in a broad range of applications such as modelling of fluids [137, 138], heat transfer and flow [139–141] or material deformation under mechanical stress [142, 143]. However, also several different quantum chemical problems have been solved with this method: SE solvers for small systems such as light atoms [129, 144–147] or diatomics [148], vibrational model systems [130] and solid state problems [149, 150]. Moreover, even Hartree-Fock [131] and DFT calculations on systems up to the size of benzene [132, 151, 152] have been performed, yielding results comparable to those obtained by the usual linear combination of atomic orbitals (LCAO) approach.

The above-mentioned publications have shown that the FEM is able to obtain reasonable results for molecular systems where the errors were comparable to those obtained with standard quantum-chemistry schemes even though their computational costs are higher. This suggests that the FEM is a good tool for computations in the field of quantum chem-

istry for going beyond the capabilities of the established schemes such as the description of unbound states.

## 4.2 Integration of Matrix Elements and Formulations of the Equation System

In section 3.5 the basics of the FEM were described and the generalised eigen system shown in equation (3.21) to solve the SE was derived. Here this is taken as starting point and a closer look at the computation of the matrix elements as well as solving strategies for the large sparse generalised eigen problems are taken.

The generalised eigenproblem as given in equation (3.21) consists of three matrices. Since the ansatz functions $\varphi_i(\boldsymbol{r})$ have only a small support, most of the matrix elements are zero. However, in two and three dimensions no distinct band structure is achievable and the matrices are irreducible. Thereby matrix elements are zero when the elements involved are not neighboured. The computation of the non-zero matrix elements involve an integration as *e.g.* the overlap integral $\mathbb{M}_{i,j} = \int d\boldsymbol{r}\varphi_i(\boldsymbol{r})\varphi_j(\boldsymbol{r})$ of ansatz functions,. Since these functions are the same for all elements, the evaluation of these integrals can be done via a lookup-table or an efficient numerical integration scheme whose required order is well-known and need only be multiplied by the Jacobian of the respective elements involved. The matrix elements $\mathbb{A}_{i,j} = \int d\boldsymbol{r}\left(\nabla\varphi_i(\boldsymbol{r})\right)\left(\nabla\varphi_j(\boldsymbol{r})\right)$ consist similar to those of $\mathbb{M}$ of overlap integrals of known functions. The only matrix containing system-specific information is the potential $\mathbb{V}_{i,j} = \int d\boldsymbol{r}\varphi_i(\boldsymbol{r})V(\boldsymbol{r})\varphi_j(\boldsymbol{r})$ which requires numerical integration by which $V(\boldsymbol{r})$ is approximated as a spline of given order.

After assembling the matrices the eigenpair $(e_i, \boldsymbol{c}_i)$ of the system

$$\left(\frac{1}{2}\mathbb{A} + \mathbb{V}\right)\boldsymbol{c}_i = e_i\mathbb{M}\boldsymbol{c}_i \tag{4.1}$$

need to be found where $e_i$ should be closest to the analytic value of the kinetic energy of the photoelectron. Since matrix eigenvalue equations with several thousands of dimensions occur in many fields, numerous schemes have been developed to solve them efficiently [153–156], a selection of them is described in section 4.5.4. Despite the numerical complexity due to the high dimensionality of this problem (several thousands of ansatz functions) the second problem is due to the fact that the eigenenergies $e_i$ are expected to be close to each other since the corresponding analytical problem has a continuous spectrum in this range. It is well known in numerics that this leads to instabilities especially for the eigen vectors, making a regularisation of the problem (described in section 4.5.3) indispensable.

## 4.3 Element Types and Mesh Types

Among the FEM formulations several 'flavours' were designed for different purposes. Given a certain equation to be solved in FEM there are in general two ways systematic ways to increase the accuracy. One way is to increase the number of elements witch is referred to as the $h$-FEM approach [41]. The refinement of the mesh is in principle always possible but technically demanding since it is not known in which regions of a mesh are too coarse

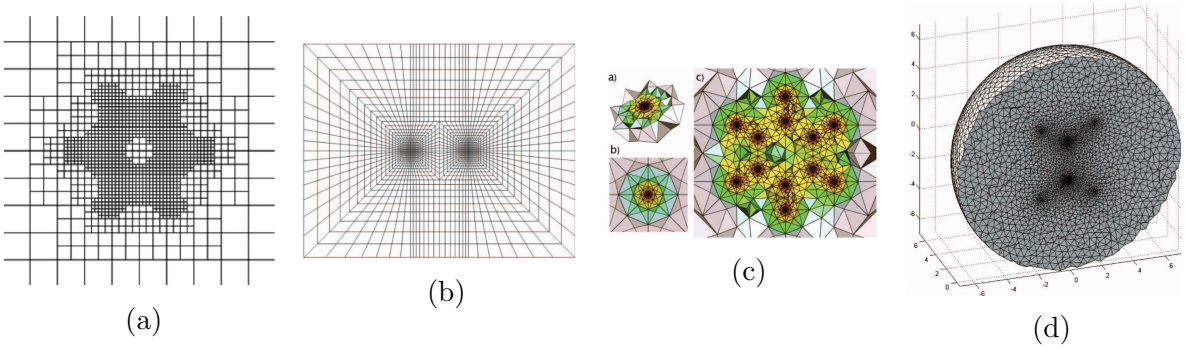


(a) (b) (c) (d)

Figure 4.1: 2D cuts through 3D meshes for molecular systems obtained with different schemes for local refinement: (a) hexahedral elements adapted for the benzene molecules [132] (b) hexahedral mesh for a diatomic [131] (c) Polyhedral mesh for a benzene geometry [151] (d) Adaptive refined tetrahedral Mesh for ethylene. [131]

in general [41]. To overcome this some FEM implementations, such as that of `Libmesh` [54] which is used here, provide an adaptive mesh refinement scheme iteratively refining the mesh using local error estimations [54]. But theses schemes are numerically demanding and hence can be only applied to benchmark systems.

The second strategy is called $p$-FEM. In the $p$-FEM scheme the order $p$ of the test functions in increased, resulting in smother and more flexible solutions. This scheme requires a large set of functions to be implemented but is known to yield good results if the function is smooth source. While standard FEM usually have only $p = 1, 2$, there are certain special-purpose schemes that go beyond this. The setup of the mesh is, as mentioned above already, critical to the quality of the solution and hence of special importance. Moreover, it is technically non trivial to set up a close packing of volume elements with the desired properties in a systematic way. There are different element types available, each with their techniques for set up. Although in principle any element shape can be chosen, in three dimensions only tetrahedral (simplex), prism- and pyramid-shaped as well as hexahedral elements commonly are used. By choosing the element shape and the polynomial order, also the type of ansatz functions is defined.

When considering meshes to describe molecular properties it is clear that the element size should be smaller in the vicinity of the nuclei while it may be broader at larger distances. One way to create a hexahedral mesh with local refinement is to start with a coarse uniform lattice and subdivide the hexahedra where necessary as shown in Figure 4.1a for a benzene molecule. Another way is to setup small regular cubic grids around the nuclei and expand them radially in boxes of growing size as shown in Figure 4.1b. These brick-shaped elements however have the disadvantages that the regular cube-like structures therein are not well-suited for atoms and molecules that rely rather on spherical shapes. Further hexahedral elements are known to give less accurate solutions than tetrahedra which are commonly used nowadays cite.

Another approach used by Lehtovaara *et al.* [151] is to put layers of polyhedra around the atoms with increasing number of points and radii. Thereby the overlapping regions of these spheres are removed by deleting elements that are closer to another atom. The mesh obtained with this procedure for a benzene molecule [132] is shown in Figure 4.1c.

When restricting oneself to tetrahedral elements, other design principles are possible: Since they are simplexes in three dimensions, they can be designed from general grids

using *e.g.* Voronoi [104] or Delaunay [157] tessellations (the latter is described in section A.1 in appendix) from a set of points with the required properties. Son and Chu [103, 107] constructed sets of points resembling molecular geometries by inserting $N$ spherical grids with different radii $r_i$ around the atoms and cutting off the overlapping regions. Thereby the respective radii are chosen as

$$r_i = \frac{il}{N - i + \frac{lN}{r_{\max}}} \qquad i = 1, \ldots, N \tag{4.2}$$

where$r_{\max}$ is the radius of the largest sphere and $l$ is a parameter smoothly changing between a linear $l \to \infty$ and a $1/r$-mapping. As spherical grids they suggested the use of Lebedev-grids [158] and a design of Womersley [159, 160]. A more detailed discussion about the choices of grids will be given in section 5.2.1.

A more entangled method is used by Alizadegan *et al.* [131]. They start with an initial guess for the wave function and create a grid whose distances are inverse proportional to the second gradient of the electron density

$$d \propto \left[ max \left\{ \left| \frac{\partial^2 \rho}{\partial^2 x} \right|, \left| \frac{\partial^2 \rho}{\partial^2 y} \right|, \left| \frac{\partial^2 \rho}{\partial^2 z} \right| \right\} \right]^{-1}.$$

which gives an estimate for the error due to linear approximation within each element. After solving the eigenvalue equation on this grid, they recompute another mesh on the basis of the new function, iterating this procedure several times. A cut through a mesh obtained by this procedure is shown in Figure 4.1d.

## 4.4 Boundary Conditions

Boundary conditions have not been addressed in this thesis so far for any of the methods but play an important role for the properties of the solution. Hence there is a large number of boundary conditions. The simplest case applicable here are Dirichlet-boundaries, requiring the wave function to vanish at the boundaries of the finite element box. In the FEM this condition can be applied especially simple by setting the coefficients of the outermost ansatz functions to zero.

Due to the large extend of the free particle, these boundaries however are unphysical if they are not applied at distances that are several times larger than the wavelength. However, considering a particle with 0.1 eV kinetic energy, its wavelength is 4.4 Angstroms and the box would need to have a diameter of several tens of Angstroms which is not feasible any more while kinetic energies in the $m$eV-range would lead to even worse scenarios.

Besides the numerical restriction to a finite box also mapping schemes can be used as *e.g.* $x = \tan(\frac{y}{2})$ that maps $[-\infty : \infty]$ to $[-\pi : \pi]$ [110]. However, using such a mapping directly is infeasible since the oscillations of the wave function would become arbitrarily sharp in the mapped range and hence the representation of the FEF would still be poor.

### 4.4.1 Complex Absorbing Potential

The complex absorbing potential (CAP) is a method often found in the literature when describing particles with infinite extent[85, 91]. In this scheme, an artificial potential usually of the form

$$W_{\mathrm{CAP}}(\boldsymbol{r}) = \begin{cases} i\nu(\boldsymbol{r}-\boldsymbol{r}_0)^2 & \boldsymbol{r} > \boldsymbol{r}_0 \\ 0 & \text{else} \end{cases} \tag{4.3}$$

is added where $\boldsymbol{r}_0$ is larger than the bound part of the system. Such a potential damps the wave function by reflecting only a small fraction of the wave back into the region of interest sources. However, studies with different shapes of these potentials show that it influences the wave function not only close to the boarders and a proper design of the parameters is....

To minimise the error due to the CAP, the parameter $\eta$ can be chosen such that its dependency on the energy vanishes in first order, *i,e.* $\eta\frac{dE}{d\eta} = 0$ [84]. Moreover, due to non-hermiticity the usual scalar product is not suitable when calculating overlap integrals any more. Too strong $\eta$ makes reflections, too weak $\eta$ lead to unstable resonances, making them strongly basis-set dependent [161]

The idea of damping down a function and making sure no reflections are scattered back to the region of interest is common to further approaches as *e.g.* absorbing boundary conditions [162], perfectly matched layer schemes [163–165] or certain variable transformations [86].

- Also read zotero: (In)FEM AbsorbBoundariesVS_InfFE

### 4.4.2 Mode-matching Schemes

Consider the solution in an inner and outer region as different variables following the equations

$$\nabla^2\Psi_1 + V(\boldsymbol{r})\Psi_1 - E\Psi_1 = 0 \qquad \nabla^2\Psi_2 - E\Psi_2 = 0 \tag{4.4}$$

whereby the outer function needs to satisfy the Sommerfeld condition $r^\alpha\left(\frac{\partial\Psi_2}{\partial r} - ik\Psi_2\right) \to 0$. These equations are coupled by the conditions

$$\Psi_1 = \Psi_2 \qquad \nabla\Psi_1\boldsymbol{n} = \Psi_2\boldsymbol{n} \tag{4.5}$$

to ensure continuity of the solution and the gradient normal to the boundary [166]. Thereby, the asymptotic behaviour of the outer function is ensured by taking ansatz functions that individually fulfil the condition and the boundaries enter the weak formulation since the application of Greens' theorem leads to an extra term.

The mode-matching scheme can be considered as a generalisation of the R-matrix approach in a finite element formulation.

### 4.4.3 The Boundary Element Method

The boundary element method (BEM) can be used as a self-standing method for solving partial differential equations using the weak formulation [167, 168]. In its pure form, the BEM solves the problems using only conditions given at its boundaries that are connected

to the volume properties via Greens' theorem, the Gauss-Ostrogradskii (divergence) theorem as well as Stokes theorem [169]. Even though the BEM procedure suffers strongly from the restriction of being applicable only to linear systems for which a fundamental solution is known as well as the disadvantage of leading to dense, unsymmetric matrix equations [168] it has some popularity until these days [170–172]. But its main advantages come into play when being used with the FEM [173] where the FEM can be used to obtain an accurate solution in the inner region and the boundaries are treated with the BEM. Considering an unbound domain as, *e.g.* the problem of the outgoing electron, the infinite domain $\Gamma$ can be divided into a finite region $\Gamma_i$ where the atoms electrostatic potential leads to ... and the remaining domain $\Gamma_o$ in which the time-independent SE reduces to the Helmholtz-problem whose fundamental solutions are well-known and thus the BEM is applicable [168, 174].

### 4.4.4 Infinite Elements

The infinite element approach was developed in the 1980-ths for acoustical caluculations and is specificly designed for the Helmholtz equation and can be understood as a advancement of the BEM that is speciallised for the Helmholtz equation. The general idea of the infinite elements is that the solution of the radial Helmholtz equation in spherical symmetry is well-known to be of the form

$$\Psi(\boldsymbol{r}) = \left(\frac{a}{r} + \frac{b}{r^2} + \dots\right) e^{ikr} \tag{4.6}$$

where $k = |\boldsymbol{k}|$ is the absolut value of the momentum of the particle and the prefactors thus correspond to different angular momenta of the outgoing electron. In the complete limit moreover, any function fulfilling the Sommerfeld radiation condition [42] can be represented.

To use this asymptotic information, in the infinite element region a layer of elements is set onto the outer surface of the finite element region in which the ansatz functions are of the form (4.6). To fulfill the continuity conditions, the front-face of these elements coincides with the outer face of the respective finite element. while their radial faces have ray-like edges with a common centre in the middle of the finite element region.

Since the first formulation of infinite elements, several different schemes were developed with increasing convergence characteristics. For brevity here only the wave-envelop formulation or Astley-Leis elements will be presented. An overwiev about different formulations is given in the references [41] and [40]. The main break-through of them is not to use the Galerkin-scheme where the ansatz- and test-functions come from the same space but to chose them of different structure. While the ansatz functions are of the form

$$\Psi(\boldsymbol{r}) = \varphi(\boldsymbol{r}) e^{ik\mu(r)}, \tag{4.7}$$

the test functions are of the shape

$$\Phi(\boldsymbol{r}) = D(r)\varphi(\boldsymbol{r}) e^{-ik\mu(r)} \tag{4.8}$$

where in three dimensions $D(r) = \frac{1}{r^2}$ [39]. With this choise of respective ansatz functions the Hamiltonian (3.22) is not symmetric anymore but still hermitian.

The functions $\varphi(\boldsymbol{r})$ are furthermore chosen to follow the product ansatz $\varphi(\boldsymbol{r}) = f(r)\varphi_2(\boldsymbol{r})$ where $\varphi_2(\boldsymbol{r})$ is an ansatz-function of a two-dimensional finite element corresponding to the inner face and for $f(r)$ Jacobi-polynomial turned out te be most stable [175].

This choise of ansatz functions has the advantage that the oscillating terms do not enter the matrix elements and due to the factor $D(r)$ the matrix elements are finite even though $\Psi(\boldsymbol{r})$ is not square-integrable. Even though the oscillating term $e^{ikr}$ cancels out, the Hamiltonian is energy dependent and thus the generalised eigenvalue problem (3.21) formulated in chapter 3.5 changes to

$$\mathbb{A}\boldsymbol{c} + ik\mathbb{B}\boldsymbol{c} - k^2\mathbb{C}\boldsymbol{c} = 0 \tag{4.9}$$

with

$$\mathbb{A}_{i,j} = \int \left( V(\boldsymbol{r})D(r)\varphi_i(\boldsymbol{r})\varphi_j(\boldsymbol{r}) - \frac{1}{2}D'(r)\varphi_i(\boldsymbol{r})\varphi_j'(\boldsymbol{r}) + \frac{1}{2}D(r)\varphi_i'(\boldsymbol{r})\varphi_j'(\boldsymbol{r}) \right) d\boldsymbol{r} \tag{4.10}$$

$$\mathbb{B}_{i,j} = \frac{1}{2}\int \left( -\mu'(r)D'\varphi_i(\boldsymbol{r})\varphi_j(\boldsymbol{r}) + D(r)(\varphi_i'(\boldsymbol{r})\varphi_j(\boldsymbol{r}) - \varphi_i(\boldsymbol{r})\varphi_j'(\boldsymbol{r})) \right) d\boldsymbol{r} \tag{4.11}$$

$$\mathbb{C}_{i,j} = \frac{1}{2}\int \left( (D(r)\mu'(r)\mu'(r) + 1)D(r)\varphi_i(\boldsymbol{r})\varphi_j(\boldsymbol{r}) \right) d\boldsymbol{r} \tag{4.12}$$

where the relation $E = \frac{1}{2}k^2$ is used [41].

This reformulation though lead to a quadratic eigenvalue problem instead of the generalised eigenvalue problem from before. However, assuming that the difference between the eigenvalues of (4.9) and the target energy of the outgoing electron is small, the quadratic eigenvalue problem can be approximated by the generalised eigenvalue problem (3.21) by setting $k$ to the respective target momentum in the Hamiltonian. However, this approximation, which is applied here for simplicity, needs to be verified.

## 4.5 Solving Large Eigenvalue Problems

In finite element applications such as those being proposed in this work, matrix equations with hundreds up to hundredthousands of dimensions need to be solved. This requries elaborate strategies, using the sparsity of these matrices.

The focus here is on solving the generalised eigenvalue problem (3.21) and the quadratic problem (4.9) respectively. However, efficient strategies are only known for regular eigenvalue problems of the form

$$\mathbb{A}\boldsymbol{x} = \lambda\boldsymbol{x}. \tag{4.13}$$

Hence, the more general forms will be rewritten to become (4.13) as discussed in the subsections 4.5.1 and 4.5.2 respectively. Moreover, since the state of interest is a free state, one needs to expect a high density of states for an appropriate mesh. This, however, is a well-known problem in numerical methematics since almost degenerate eigenvalues are very sensitive to small perturbations and their respective eigenvectors even more. Though

the subsection 4.5.3 addresses these problems and a way for numerical stabilisation is sketched.

Finally in the subsection 4.5.4 a few methos are presented showing how a small number of approximate eigenpairs can be obtained in a numerically efficient way from the usual eigenproblem (4.13).

How is this inversion done numerically?

### 4.5.1 Quadratic Eigenproblem

–¿ Probably this chapter is not of interest here since I don't use the respective formulation!?

### 4.5.2 Generalised Eigenproblem

The most straight-forward way to reformulate the generalised eigenvalue problem

$$\mathbb{A}\boldsymbol{x} = \lambda\mathbb{B}\boldsymbol{x}, \tag{4.14}$$

is te invert the matrix $\mathbb{B}$, obtaining the regular Eigenproblem $\mathbb{B}^{-}1\mathbb{A}\boldsymbol{x} = \lambda\boldsymbol{x}$. This way is possible as long as $\mathbb{B}$ is invertable and not too large since inversion is a demanding task and the resulting matrix is not sparse anymore [176].

To prevent the use of dense matrices, libraries often do not operate with the matrices themselves but rather with a set of vector on which these matrices act [176]. The most popular scheme of this kind is the Rayleigh-Ritz projection where the initial problem is approximated on a small subspace $\mathcal{V}_j = span\{\boldsymbol{v}_1, \ldots, \boldsymbol{v}_j\}$, spanned by appropriate vectors $\boldsymbol{v}_i$.

Projecting the original problem (4.14) onto this subspace yields the new system $\mathbb{\Sigma}_j\boldsymbol{s} = \theta\mathbb{\Theta}_j\boldsymbol{s}$ where $\mathbb{\Sigma}_j = \mathbb{V}_j^T\mathbb{A}\mathbb{V}_j$ and $\mathbb{\Theta}_j = \mathbb{V}_j^T\mathbb{B}\mathbb{V}_j$ respectively which is only of dimensionality $j$. The matrix $\mathbb{V}_j$ is unitary with the rows $(\mathbb{V}_j)_i = \boldsymbol{v}_i$. After solving this dense but small problem, the original eigenvectors can be approximated as $\boldsymbol{x}_j = \mathbb{V}_j\boldsymbol{s}_j$ and $\lambda = \theta_j$. The obtained eigenpair is a good approximation to the actual one as long as the subspace $\mathcal{V}_j$ contains the respective solution or contains a vector which is at least close to it. A commonly used approach the Krylov subspace.

### 4.5.3 Stabilisation of Eigenproblems

Independent of the efficiency and robustness of the eigensolver in use, seeking solutions of the SE for free particles means that eigenpairs are to be found whose energies are, if the numerical parameters are chosen well, very dense or even degenerate. Unfortunately, dense-lying eigenvalues lead to numerical difficulties; especially the eigenvectors are known to be unreliable in this case. In practice, this means that the iterative schemes do not converge anymore, requireing a reformulation of the mathematical probelm.

One way to circumvent the instabilities in the original problem (4.14) is to reformulate it as a minimisation problem [25]. Therefore equation (4.1) is rewritten as $\left(\frac{1}{2}\mathbb{A} + \mathbb{V} - \varepsilon\mathbb{M}\right)\boldsymbol{c}_i = 0$ where $\varepsilon$ is the target energy. Since this will have most likely no unambiguous solution,

one minimises the residuum

$$\min_{||\boldsymbol{x}||=1} \left\{ \left| | \left( \frac{1}{2}\mathbb{A} + \mathbb{V} - E\mathbb{M} \right) \boldsymbol{x} \right| | \right\}. \tag{4.15}$$

Using the $L_2$-norm, this is the same as finding the smallest eigenvalue of

$$\left( \frac{1}{2}\mathbb{A} + \mathbb{V} - E\mathbb{M} \right)^{\dagger} \left( \frac{1}{2}\mathbb{A} + \mathbb{V} - E\mathbb{M} \right) \boldsymbol{x}_i = \theta \boldsymbol{x}_i \tag{4.16}$$

where $\theta$ is a measure for the error in energy. To avoid the costly multiplication of two matrices, one can use Hermiticity of the matrices and take compute the square root as

$$\left( \frac{1}{2}\mathbb{A} + \mathbb{V} - E\mathbb{M} \right) \boldsymbol{c}_i = \lambda \boldsymbol{c}_i \tag{4.17}$$

which is a usual eigenvalue problem [25] and $\lambda$ with smallest absolute value is searched.

Nonetheless, the latter formulation is only an approximation as the comparison of (4.14) and (4.17) shows, the latter approximates the mass matrix$\mathbb{M}$ as unity $\mathbb{1}$. Furthermore, equation (4.17) still is expected to have a very dense spectrum and $\lambda$ is an interior eigenvalue so the initial problem is not expected to be solved in this approach.

Instead of the reformulation, here a regularisation of the problem used, applying the spectral transformation shift and invert. Starting thit the problem: $\mathbb{A}\boldsymbol{x} = \lambda\mathbb{B}\boldsymbol{x}$ where the eigenvalues closest to the target energy $\varepsilon$ are of interest, the spectrum can be shifted to a target energy of 0 by

$$(\mathbb{A} - \varepsilon\mathbb{B})\, \boldsymbol{x} = (\lambda - \varepsilon)\mathbb{B}\boldsymbol{x} \tag{4.18}$$

and than inverted to become

$$\boldsymbol{x} = (\lambda - \varepsilon)\, (\mathbb{A} - \varepsilon\mathbb{B})^{-1}\, \mathbb{B}\boldsymbol{x} \tag{4.19}$$

which is equivalent to the usual eigenproblem

$$(\mathbb{A} - \varepsilon\mathbb{B})^{-1}\, \mathbb{B}\boldsymbol{x} = \tilde{\lambda}\boldsymbol{x} \qquad \tilde{\lambda} = \frac{1}{\lambda - \varepsilon}. \tag{4.20}$$

The formulation (4.20) has the advantage that the transformed eigenvalues are well-separated and on the extrema of the new spectrum, making the convergence faster and more stable [177].

- Why do I prefer to use the first formulation?
- Computing Interior Eigenvalues with Harmonic Extraction –¿ still good/nice with ST?
- Purification of Eigenvectors –¿ Can it help me to do some nice shit?

### 4.5.4 Solving Large Eigenproblems

For the computation of eigenpairs large classes of solvers have been developed with various numerical properties. Besides direct solvers such as the Gauß-elimination, many iterative solvers have been developed that are especially well-suited for large but spares problems. Besides the famous Jacobi- and Gauß-Seidel algorithms which converge only in certain

cases, also the Davidson method and several Krylov subspace methods are commonly used.

As discussed in the sections 4.5.2 and 4.5.3 already, the solution of a generalised eigenvalue problem involves matrix operations which need to be avoided to keep their sparse structure.

As a popular choise for such classes of problems, the Krylov subspace is used. An $r$-dimensional Krylov subspace is generated by a vector $\boldsymbol{x}$ and a matrix $\mathbb{A}$ and has the form

$$\mathcal{K}_r(\mathbb{A}, \boldsymbol{x}) = span\left\{\boldsymbol{x}, \mathbb{A}\boldsymbol{x}, \mathbb{A}^2\boldsymbol{x}, \ldots, \mathbb{A}^{r-1}\boldsymbol{b}\right\}. \tag{4.21}$$

If $\mathbb{A}$ is sparse, the evaluation of these expressions is only of order $\mathcal{O}(d)$ where $d$ is the dimensionality of $\boldsymbol{x}$. The vectors obtained with large powers of $\mathbb{A}$ however usually become more and more linearly dependent. To prevent this, the vectors usually are orthonormalised subsequently.

An important issue in this scheme is a good choise for $\boldsymbol{x}$ which crucially determines the speed of convergence. If a reasonable start-vector is not given, the space $\mathcal{K}_r$ needs to be extended by increasing $r$ iteratively. The orthogonalisation method being used distinguishes different Krylov subspace methods such as the Arnoldi [178] or Lanczos [179]. In the particular implementation, the Krylov-Schur algorithm is used [177] which was introduced 2001 [180]. To keep the dimensionality low, most schemes restart the algorithm after $r$ reached a certain value, starting with a better guess $\boldsymbol{x}$. The efficient restart is another critical issue in this scheme. In the Krylov-Schur algorithm [180] used here, the restart is conducted implicitly as described in more detail in ref. [177].

# 5 | Computational Details

After describing different approaches to compute PESs and pointing out why the Dyson orbital formalism combined with a finite element method used to calculate the photoelectron function is well-suited for our needs, in this chapter now the protocol as being used to obtain the PESs will be presented.
In the first section, the computation of the initial (unionised) and final (ionised) states will be described. Thereafter, in section 5.2.1 the setup of the finite element system used to compute the free electron function as well as the dipole matrix element will be described. In the final section, the computation of Dyson orbitals will be sketched and it will be described how to transfer it to the finite element setup.

## 5.1 Bound State Functions

The formalism as it was described in 2.3 can be used with any quantum chemical method that is able to calculate ground and excited state wave functions and respective energies. Since density functional theory (DFT) and its time dependent counterpart TDDFT have shown to be accurate and numerically cheap methods, we use these methods here.

It is based on the Hohenberg-Kohn theorem [43] which states that the ground-state electron density determines the potential in the SE uniquely and with this also the wavefunction. Thus, the electron density contains all information about a given system. Since it does not point to a way how to determine the electron density without knowing the wavefunction, usually the Kohn-Sham scheme [44] is used where the electrons are described non-interacting particles in a respective pseudo-potential that is made such that the electron density of these Kohn-Sham orbitals corresponds to the real electron density. Since the particles do not interact with each other, the Kohn-Sham orbitals $\Psi_j(\boldsymbol{r})$ are solutions to the partial differential equation

$$\left(-\frac{1}{2}\nabla^2 + V_{\text{eff}}(\boldsymbol{r})\right)\Psi_j(\boldsymbol{r}) = \epsilon_j \Psi_j(\boldsymbol{r}) \tag{5.1}$$

where $\epsilon_j$ is the binding energy of the respective electron and the effective potential

$$V_{\text{eff}}(\boldsymbol{r}) = V_{\text{ext}}(\boldsymbol{r}) + \int \frac{\rho(\boldsymbol{r}')}{|\boldsymbol{r}-\boldsymbol{r}'|} d\boldsymbol{r}' + V_{\text{xc}}(\boldsymbol{r}) \tag{5.2}$$

can be separated into the external potential $V_{\text{ext}}(\boldsymbol{r})$ which consists of the attractive nuclear electrostatic potential. The second term is the electrostatic interaction of the electrons. With these contributions, this formalism is on the level of theory of the Hartree-theory,

missing the exchange and correlation. The respective contributions are put in $V_{\mathrm{xc}}(\boldsymbol{r})$ together with the error in kinetic energy due to the fact that the single-electron functions of the Kohn-Sham scheme differ from the real electrons and thus have an other kinetic energy as well [181]. About the latter not much is known except that it is non-local, that means its value at $r$ depends on the electron densities at all other places as well. The main callenge in DFT is to find an appropriate approximation to this functional.

Add something how to get excited-state properties?

In this work the calculations are done using a locally modified version of the program package `NWChem` [52] where a more verbose output enables the reconstruction of all molecular orbitals and thus the computation of the DOs.

### 5.1.1 OTRSH-scheme

One main issue concerned with the DFT-formalism is that the approximate exchange functional decays exponentially instead of $\frac{1}{r}$ and $\frac{1}{r^4}$ for the exchange and correlation terms respectively. This wrong behaviour affects the obtained wave functions and thus the orbital energies [45].

To reduce this error, so-called range-separated hybrid (RSH) functonals are used, in which the DFT-exchange term is used for small interelectronic distances only, while at larger distances, where correlation effects are not that important, the Hartree-Fock excact-exchange is used. The interchange between the schemes is done by the separation

$$\frac{1}{r} = \frac{\alpha + \beta erf(\omega r)}{r} + \frac{1 - \alpha - \beta erf(\omega r)}{r} \tag{5.3}$$

where $\alpha + \beta = 1$ and $\beta$ are parameters to be chosen. Besides taking the standard parameters, an ab-initio scheme to chose them is the optimally-tuned RSH (OTRSH) scheme where the functional

$$J(\alpha_{\mathrm{opt}}, \omega_{\mathrm{opt}}) = min_{\alpha,\omega} \{|E_N(\alpha, \omega) - E_{N-1}(\alpha, \omega) - \varepsilon_{\mathrm{HOMO}}|\} \tag{5.4}$$

is minimised, making sure that Koopman's theorem is fulfilled [45]. Besides similar functionals which account for the electron affinities or ionisation potentials of lower-lying orbitals, the optimisation according to stability or the most-straight line of partial charges can be chosen as equivalent ab-initio criteria. More details on these schemes? Not mention them at all?

For this optimization procedure the Gaussian package `G09` [53] is used with the 6-31G(d) [182, 183] basis set and the functional LC-BLYP [184]. The ground state DFT calculation, determination of geometries and the linear-response TDDFT calculations have been conducted with a locally modified version of `NWChem` [52], employing the basis set def2-tzvp [185] without symmetry restrictions. The Kohn-Sham orbitals (obtained by ground state DFT) and CI-coefficients (obtained by linear-response TDDFT which yields the configuration interaction singles expansion for a number of excited states) as well as the atomic overlap matrix are interfaced to the in-house software `DYSON` [31] that computes the DOs. The integration of the overlap matrix in eq. (**??**) finally is perfomed using `ezDyson` [33].

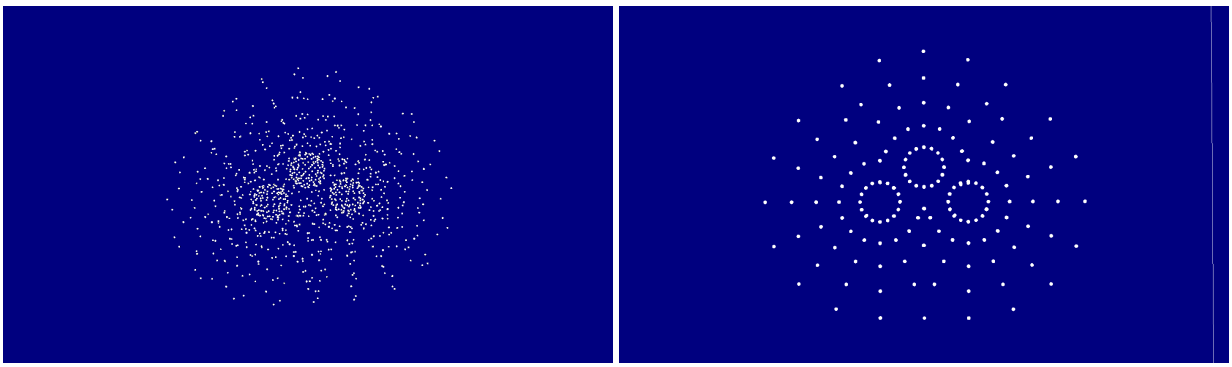

Figure 5.1: Example of a mesh for the water-geometry. It consists of 5 spheres with constant number of points per sphere. The overlapping regions are cut off. Left: cut through the nuclear plane.

### 5.1.2 Computing the Dyson orbital

The DO is computed in the framework of this thesis with the in-house code `DYSON` [31].

## 5.2 Free electron function

The FEF is computed with a finite element scheme, using the program `Free Willy` developed in the framework of this thesis. It is based on the library `Libmesh` [54] which itself uses sevaral libraries for the required linear algebra and the mesh-setup.

### 5.2.1 Setup of the Grid

The most crucial part of the FEM is the mesh under usage. In the program `FreeWilly` it is obtained from a set of points via Delaunay triangulation (see A.1 for details) using the library `tetgen` [186]. The distribution of these points is responsible for the quality of the obtaind solution and depends on many parameters in a non-trivial way. The dependence is in particular on

**The molecular geometry** Close to the cores it should be denser, at larger distances a coarser grid is possible.

**The kinetic energy** of the photo electron which gives the maximum distance between two points

**The largest angular momentum of the Dyson orbital** determines the angular momentum of the photoelectron to be resembled.

In the general scheme the generation of the point-distribution follows the suggestion of Son and Chu [107]: The grid is set up of atomar grids, *e.g.* spherical distributions, each centered at atoms where the overlapping regions are cut off. The radii of these spheres needs to be much larger than the bond lengthes, holes or interatomic gaps in the molecule to (*e.g.* holes in aromatic rings or the space between ligands of larger molecules). Using this scheme, the grid-parameters are determined by the size of the larges box $r_{\max}$, number $N$ of spheres used as well as the radial distribution of them and the angular distribution of points on these spheres.

For the radial distribution Son and Chu [103] suggested the scheme

$$r_i = \frac{il}{N - i + \frac{lN}{r_{\max}}} \qquad i = 1, \ldots, N \tag{5.5}$$

where $l$ is a parameter to chose. As an alternative distribution, here the formula

$$r_i = \frac{il}{\left(\frac{N}{i}\right)^p \left(\frac{Nl}{r_{\max}} - 1\right) + 1} \qquad i = 1, \ldots, N \tag{5.6}$$

is to be tested where $l$ and $p \geq 1$ are parameters to chose whereby the condition $N < \frac{r_{\max}}{l}$ should be fulfilled to prevent the singularity.

While the distribution of spheres follows, at least on a qualitative level, a clear scheme since it should always resemble the local kinetic energy, the distribution on the surface of each sphere is not that clear. Qualitatively it is preferable to chose a regular grid but this more challenging. Since the ... grid, which is known from the ... is clearly a bad choise due to its high density close to the poles, in geological applications often so-called geodesic grids are chosen.

Some explanations are given here:
- Lebedev-grid -¿ try to get spherical harmonics with highest L accurate.
-If also required: all weights should be equal: spherical t-designs.
Leads directly to the question of uniform distribution.-¿ not directly by algorithms
- other approach: close packings
- energy minimisation: Consider nodes as interacting particles -¿ minimise E for some model potential.
see http://people.maths.ox.ac.uk/beentjes/Essays/QuadratureSphere.pdf. - crude but fast algorithms Since in finite element theory the sphere neither needs to be really round nor is there any global functional defined on it, the complicated distributions described above may be not even needed. An other approach therefore is to use an algorithm that gives just a more or less uniform distribution.

Approach used for climate models: so-called geodesic grids: subdivision of polyhedra, projected onto the sphere[187, 188], see also for further information.

The point sets I took are from here: [189, 190].

The above mentioned techniques show the large variety of different approaches and it is not very clear which one will meet our needs best. Moreover, here the problem is not only two dimensional but the whole sphere (not only its surface) needs to be subdivided. Hence, besides the question of a radial density of different spherical surfaces, also the number of points per sphere as function of the radial distance needs to be considered.

Whether the approach of subdividing the atomic meshes into radial and angular parts as opposed to another volume tessellation can be questioned and may turn out to be inefficient. Application of Geodesic grid in calculating surface charges: [191], also mentioning Connolly algorithm (refs 26, 29 therein).

The second scheme has a divergence around $Nl = r_{\max}$. It can be shown that the condition $N \leq \frac{r}{l}$ is enough here to stabilise it.

If the above described procedures prove to be too inefficient, one could try to implement some WKB-based scheme similar to [112] but in 3D. Thereby, the number of points in a

given volume element is determined by $N_i = \frac{\alpha_i}{\alpha} N$ where $\alpha = \sum_i \alpha_i$ and

$$\alpha_i = \int_V dV \sqrt{2\mu(E - V(r))}$$

.This ensures dense points there, where the potential is lowest and a coarse mesh far away; however, a consistent formulation in 3D would need to be invented.

To account for the molecular geometry and the general tendency of the photo electron to oscillate stronger in the vicinity of the nuclei, the mesh is built out of spheres, centred at the nuclear positions. Thereby, a study of Son [103] had shown that it is numerically most efficient when the overlapping regions of these spheres are cut out. Figure 5.1 shows an example for the water molecule.
For the radial distribution we will use the the function

$$r_i = \frac{1 + x_i}{1 - x_i + \frac{2L}{r_{max}}} L \qquad x_i = \frac{2i}{N_r} - 1$$

suggested by Son *et. al.*[103, 107]. The parameters $N_r$, $L$ specifying the number of spheres and their distribution; the larger $L$ is, the denser are the spheres close to the centre.
The optimal choise of these parameters as well as the angular distribution of points on the spheres is still an open quetion. Finally, after putting the points together as described above, they are connected to a Delaunay triangulation using `tetgen` [186]. Here additional points may be introduced to guarantee well-shaped elements (`i.e.` no sharp peaks). one scheme suggested by Son and Chu [103]:

$$r_i = \frac{il}{N - i + \frac{lN}{r_{\max}}} \qquad i = 1, \ldots, N$$

where $l$ is a parameter to chose. Own scheme:

$$r_i = \frac{il}{\left(\frac{N}{i}\right)^p \left(\frac{Nl}{r_{\max}} - 1\right) + 1} \qquad i = 1, \ldots, N$$

where $l$ and $p \leq 1$ are parameters to chose. Thereby it is important to mention that in this scheme (in contrast to the above one) the (asymptotic for $r \to \infty$) maximum distance between two spheres is $l$ and hence could be physically chosen to $l \approx \frac{\lambda}{2}$.
The second scheme has a divergence around $Nl = r_{\max}$. It can be shown that the condition $N \leq \frac{r}{l}$ is enough here to stablilise it.

Besides the tricky question about this mapping, also the number of points per sphere depending on the radial distance should be considered. In [103] this is chosen to be constant without further discussion but of course there are several possible design criteria as well. Besides a constant number, also a constant spherical density (hence $N \propto r^2$) are possible; However, it might be sensible to follow a similar idea than in the radial mapping: Being fine close to the nuclei and get coarser with increasing distance. In particular, I followed the design rule of keeping the space between points in radial direction similar to space between points in angular distribution. Hence, $d_{\text{spheric}} = \sqrt{\frac{4\pi r_i^2}{N_i}} \approx r_i - r_{i-1}$. For the

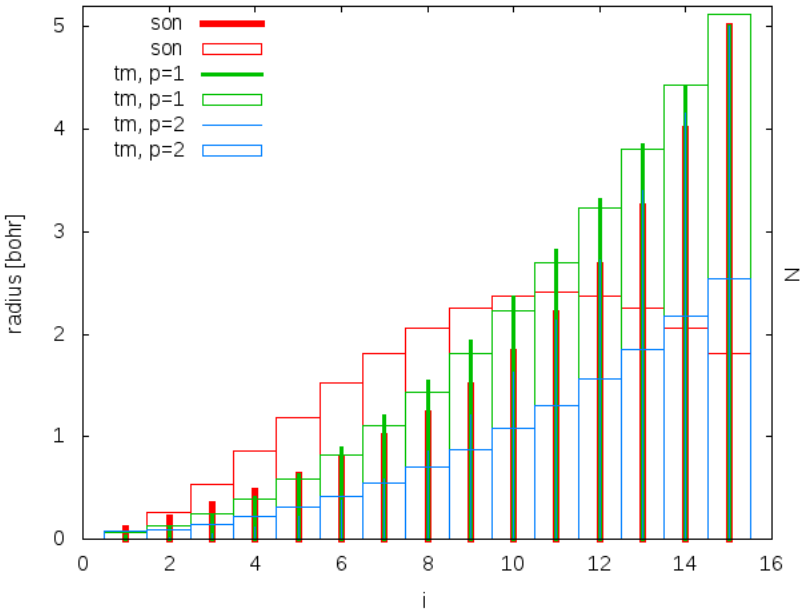


Figure 5.2: the radius and number of points of the spheres as for $N = 15$, $r_{\max} = 5$ and $l = 2$.

above described radial schemes, this results in

$$N_i = \frac{4\pi}{\left(1 - \frac{i-1}{i}\frac{N-i+\frac{lN}{r_{\max}}}{N-i+1+\frac{lN}{r_{\max}}}\right)^2}$$

for the first scheme and

$$N_i = \frac{4\pi}{\left(1 - \frac{i-1}{i}\frac{(\frac{N}{i})^p\left(\frac{lN}{r_{\max}}-1\right)+1}{(\frac{N}{i-1})^p\left(\frac{Nl}{r_{\max}}-1\right)+1}\right)^2}$$

for the latter.
The respective radii and number of points per sphere are shown in figure 5.2.
Special mapping schemes are the constant radial mapping $r_i = ai$ which corresponds to a constant spherical grid density $N_i = 4\pi a^2 i^2$ and an exponential map $r_i = q^i r_0$ which would require a constant number of spherical grid points $N_i = \frac{4\pi q^2}{(1-q)^2}$ according to the rule derived above.

Since some of the spherical schemes described above allow only for certain numbers of points each, here, the best approximation is used respectively.

### 5.2.2 Benchmark

Tested on Lithium with a sphere with $r_{\max} = 2.8$ 1: Using the mapping of Son with a naive approach, setting the number of circles by hand and growing quadratically with the size ($N_{\text{circle}} = 20$, $l = 2.0$ , $N = 10$) 2: using the Son scheme with N according to above formula 3: using the tm scheme as described above, p=1 4: using the tm scheme as described above, p=2

| scheme | #elements | error in energy [a.u.] |
|---|---|---|
| 1 | 2370 | 0.496220, 0.520199, 0.572279 |
| 2 | 2022 | 0.038136, 0.046119, 0.055691 |
| 3 | 2166 | -0.003638, 0.027219, 0.050588 |
| 4 | 2338 | none converged |

Thereby, the number of elements were kept as similar as possible.

### 5.2.3 Obtaining ESP

- obtained from `NWChem` - interpolation of that grid

## 5.3 Obtaining the DOs

- from coefficients to values

# 6 | Results

Showing PES: - benzene - near-threshold PES - Find systems where PES is known for different photon energies

There is a paper[192] with vibronically resolved PES from experiment.
PES of N2 with 'angular resolution' (latter not directly) [193].

purine and pyrimidine: comparison to Green's function methods via the [60]-paper.

For $AlO^-$ there is a paper with 2 spectra with one and two transitions each, having vibrational structure[194].

Atomic Systems have some experimental data as well: For Xe and Kr the spectra at photon energies of 150 eV are shown in reference [195].

A combined theoretical and experimental study on $CH_2F_2$ is in ref. [196]. Here, theory is quite bad and experiment is also angular resolved, thus may be interesting.

## 6.1 atomic Lithium

As the smallest system that has multiple electrons in its anionic state as well, Lithium is an important test object that has theoretical as well as experimental reference data available[73, 74, 197]. Experiment from Moore, cited in [197]; original not found. Experiment 2 from [30].

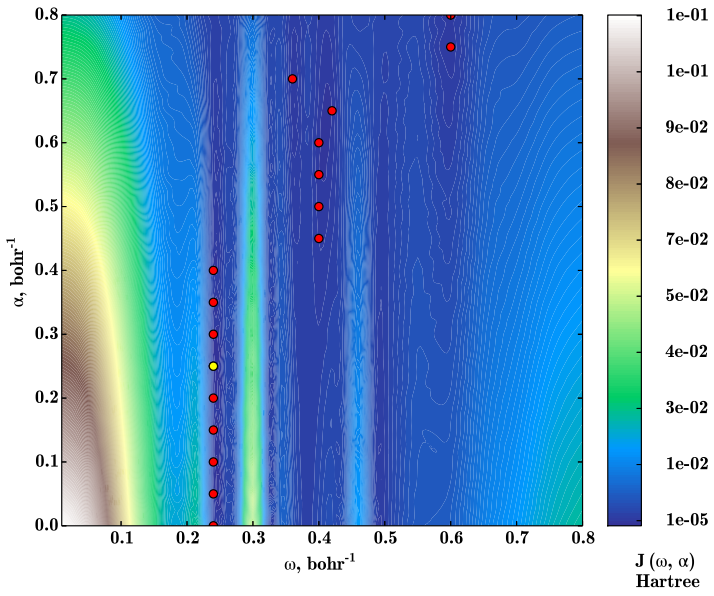


Figure 6.1: The functional $J(\alpha, \omega)$ described in eqation (5.4) for Lithium

The appearance of $2p$-states are accessed by a dipole-transition in the bound part and can not be described within the theory applied here due to the neglect of the conjugate DO term in equation (2.14) [93].

## 6.2 Triatomic Linear Molecules

There are several studies on $CO_2$ [198–201], $CS_2$ [200, 201], COS [200, 201] and $N_2O$ [201]

$CS_2$ is known to have strong correlation effects [65]

## 6.3 water

The PES and threshold PES, where the kinetic energy of the photoelectron is kept constant instead of the energy of the photon, of water is experimentally well studied for different photon energies. As example, in Ref. [202] the PES of water and several TPES of water and heavy water are investigated with high resolution.
Similar high accuracy is achieved in Ref. [203] where the PES of $H_2O^+$ and $D_2O^+$ are studied with a He1 source, radiating at 537 Angs.
Further PES are available at higher photon energies: In [204], photons at energies of 1200 eV are used. A further study of Winter *et. al.* measured spectra at 60, 75 80, 100 and 120 eV in gas and liquid phase [1].
These studies are of interest here since they yield a variety of different test-cases on a single system that can be used to prove the method being used to be valid.

# 7 | Resumee

- is it worth the effort? - What energy-range is achievable? - Which effects are still missing?

- How to proceed with it?

# Bibliography


[1] B. Winter et al. "Full Valence Band Photoemission from Liquid Water Using EUV Synchrotron Radiation". In: *The Journal of Physical Chemistry A* 108.14 (Apr. 2004), pp. 2625–2632. DOI: 10.1021/jp030263q.

[2] Kathrin M. Lange and Emad F. Aziz. "The Hydrogen Bond of Water from the Perspective of Soft X-Ray Spectroscopy". In: *Chemistry – An Asian Journal* 8.2 (2013), pp. 318–327. DOI: 10.1002/asia.201200533.

[3] Sophie E. Canton et al. "Visualizing the non-equilibrium dynamics of photoinduced intramolecular electron transfer with femtosecond X-ray pulses". In: *Nature Communications* 6.6359 (Mar. 2015). DOI: 10.1038/ncomms7359.

[4] Benjamin E. Van Kuiken and Munira Khalil. "Simulating Picosecond Iron K-Edge X-ray Absorption Spectra by ab Initio Methods To Study Photoinduced Changes in the Electronic Structure of Fe(II) Spin Crossover Complexes". In: *The Journal of Physical Chemistry A* 115.39 (2011). PMID: 21846088, pp. 10749–10761. DOI: 10.1021/jp2056333. eprint: http://dx.doi.org/10.1021/jp2056333.

[5] Xin Yang et al. "Solvation of the Azide Anion (N3-) in Water Clusters and Aqueous Interfaces: A Combined Investigation by Photoelectron Spectroscopy, Density Functional Calculations, and Molecular Dynamics Simulations". In: *The Journal of Physical Chemistry A* 108.39 (2004), pp. 7820–7826. DOI: 10.1021/jp0496396. eprint: http://dx.doi.org/10.1021/jp0496396.

[6] Babak Minofar et al. "Interior and Interfacial Aqueous Solvation of Benzene Dicarboxylate Dianions and Their Methylated Analogues: A Combined Molecular Dynamics and Photoelectron Spectroscopy Study". In: *The Journal of Physical Chemistry A* 109.23 (2005), pp. 5042–5049. DOI: 10.1021/jp050836u. eprint: http://dx.doi.org/10.1021/jp050836u.

[7] Stephan Thürmer et al. "Flexible H2O2 in Water: Electronic Structure from Photoelectron Spectroscopy and Ab Initio Calculations". In: *The Journal of Physical Chemistry A* 115.23 (2011). PMID: 21332235, pp. 6239–6249. DOI: 10.1021/jp111674s. eprint: http://dx.doi.org/10.1021/jp111674s.

[8] Mihajlo Etinski and Christel M. Marian. "Ab initio investigation of the methylation and hydration effects on the electronic spectra of uracil and thymine". In: *Phys. Chem. Chem. Phys.* 12 (19 2010), pp. 4915–4923. DOI: 10.1039/B925677F.

[9] Franck Lépine, Giuseppe Sansone, and Marc J.J. Vrakking. "Molecular applications of attosecond laser pulses". In: *Chem. Phys. Lett.* 578 (July 18, 2013), pp. 1–14.

[10] Eleftherios Goulielmakis et al. “Real time observation of valence electron motion”. In: *Nature* 466 (Aug. 5, 2010), pp. 739–744. DOI: 10.1038/nature09212.

[11] Dr. Giuseppe Sansone et al. “Electron Correlation in Real Time”. In: *Chem. Phys. Chem.* 13.3 (2012), pp. 661–680. DOI: 10.1002/cphc.201100528.

[12] Matthias F. Kling and Marc J.J. Vrakking. “Attosecond Electron Dynamics”. In: *Annual Review of Physical Chemistry* 59.1 (May 2008), pp. 463–492. DOI: 10.1146/annurev.physchem.59.032607.093532.

[13] M. Uiberacker et al. “Attosecond real-time observation of electron tunnelling in atoms”. In: *Nature* 446.7136 (Apr. 5, 2007), pp. 627–632. DOI: 10.1038/nature05648.

[14] Ferenc Krausz and Misha Ivanov. “Attosecond physics”. In: *Reviews of Modern Physics* 81.1 (Feb. 2, 2009), pp. 163–234. DOI: 10.1103/RevModPhys.81.163.

[15] T Koopmans. “Über die Zuordnung von Wellenfunktionen und Eigenwerten zu den Einzelnen Elektronen Eines Atoms”. In: *Physica* 1.1 (1934), pp. 104–113. DOI: http://dx.doi.org/10.1016/S0031-8914(34)90011-2.

[16] C.-O. Almbladh and U. von Barth. “Exact results for the charge and spin densities, exchange-correlation potentials, and density-functional eigenvalues”. In: *Phys. Rev. B* 31 (6 Mar. 1985), pp. 3231–3244. DOI: 10.1103/PhysRevB.31.3231.

[17] David A. Egger et al. “Outer-valence Electron Spectra of Prototypical Aromatic Heterocycles from an Optimally Tuned Range-Separated Hybrid Functional”. In: *JCTC* 10.5 (2014), pp. 1934–1952. DOI: 10.1021/ct400956h.

[18] Thomas Körzdörfer et al. “Assessment of the performance of tuned range-separated hybrid density functionals in predicting accurate quasiparticle spectra”. In: *Phys. Rev. B* 86 (20 Nov. 2012), p. 205110. DOI: 10.1103/PhysRevB.86.205110.

[19] T. Körzdörfer et al. “When to trust photoelectron spectra from Kohn-Sham eigenvalues: The case of organic semiconductors”. In: *Phys. Rev. B* 79 (20 May 2009), p. 201205. DOI: 10.1103/PhysRevB.79.201205.

[20] C-Z Gao et al. “On the dynamics of photo-electrons in C 60”. In: *J Phys. B-A. Mol. Opt.* 48.10 (2015), p. 105102.

[21] Yu. N. Zhuravlev and D. V. Korabelnikov. “The nature of the electronic states and photoelectron spectra of oxyanion crystals”. In: *Journal of Structural Chemistry* 50.6 (2009), pp. 1021–1028. DOI: 10.1007/s10947-009-0151-7.

[22] R. Leckey. “Ultraviolet Photoelectron Spectroscopy of Solids”. In: *Surface Analysis Methods in Materials Science*. Ed. by D. John O’Connor, Brett A. Sexton, and Roger St. C. Smart. Berlin, Heidelberg: Springer Berlin Heidelberg, 1992, pp. 291–300. DOI: 10.1007/978-3-662-02767-7_14.

[23] J Schirmer et al. “Break-down of the molecular-orbital picture of ionization: CS, PN and P 2”. In: *Journal of Physics B: Atomic and Molecular Physics* 11.11 (1978), p. 1901.

[24] J. Schirmer et al. “Strong Correlation Effects in inner Valence Ionization of N2 AND CO”. In: *Chemical Physics* 26.1 (1977), pp. 149–153. DOI: http://dx.doi.org/10.1016/0301-0104(77)87101-2.

[25] M. Brosolo and P. Decleva. “Variational approach to continuum orbitals in a spline basis: An application to H2+ photoionization”. In: *Chemical Physics* 159.2 (Jan. 1992), pp. 185–196. DOI: 10.1016/0301-0104(92)80069-8.

[26] A. Abdurrouf and F. H. M. Faisal. “Theory of intense-field dynamic alignment and high-order harmonic generation from coherently rotating molecules and interpretation of intense-field ultrafast pump-probe experiments”. In: *Phys. Rev. A* 79 (2 Feb. 2009), p. 023405. DOI: 10.1103/PhysRevA.79.023405.

[27] Peng Zhang and A. G. R. Thomas. “Enhancement of high-order harmonic generation in intense laser interactions with solid density plasma by multiple reflections and harmonic amplification”. In: *Applied Physics Letters* 106.13 (Mar. 30, 2015), p. 131102. DOI: 10.1063/1.4916739.

[28] B. Dromey et al. “High harmonic generation in the relativistic limit”. In: *Nature Physics* 2.7 (July 2006), pp. 456–459. DOI: 10.1038/nphys338.

[29] Enrico Fermi. *Nuclear Physics*. Chicago: University of Chicago Press, 1949.

[30] B. Sonntag and P. Zimmermann. “XUV spectroscopy of metal atoms”. In: *Reports on Progress in Physics* 55.7 (1992), p. 911.

[31] Gilbert Grell. “Theoretical Study of X-Ray Photoelectron Spectroscopy of Transition Metal Complexes”. University of Rostock, 2015.

[32] L. D. Landau and E.M. Lifschitz. *Quantenmechanik*. 9th ed. Berlin: Akademie-Verlag, 1979.

[33] C. Melania Oana and Anna I. Krylov. “Cross sections and photoelectron angular distributions in photodetachment from negative ions using equation-of-motion coupled-cluster Dyson orbitals”. In: *J. Chem. Phys.* 131.12, 124114 (2009). DOI: http://dx.doi.org/10.1063/1.3231143.

[34] Yuan Liu and Chuangang Ning. “Calculation of photodetachment cross sections and photoelectron angular distributions of negative ions using density functional theory”. In: *The Journal of Chemical Physics* 143.14 (Oct. 14, 2015), p. 144310. DOI: 10.1063/1.4932978.

[35] Dietrich Braess. *Finite Elemente*. 4th ed. Heidelberg: Springer, 2007.

[36] David Gilbarg. *Elliptic Partial Differential Equations of Second Order*. Berlin: 1983, 1983.

[37] Philippe G. Ciarlet. *The Finite Element Method for Elliptic Problems*. Amsterdam et al.: SIAM, 2002.

[38] R. J. Astley. “Wave envelope and infinite elements for acoustical radiation”. In: *International Journal for Numerical Methods in Fluids* 3.5 (1983), pp. 507–526.

[39] R. J. Astley et al. “Three-dimensional wave-envelope elements of variable order for acoustic radiation and scattering. Part I. Formulation in the frequency domain”. In: *The Journal of the Acoustical Society of America* 103.1 (1998), pp. 49–63.

[40] R. J. Astley. “Infinite elements for wave problems: a review of current formulations and an assessment of accuracy”. In: *International Journal for Numerical Methods in Engineering* 49.7 (2000), pp. 951–976.

[41] Daniel Dreyer. “Efficient Infinite Elements for Exterior Acoustics”. PhD thesis. Germany: TU Hamburg-Harburg, 2004.

[42] A. Sommerfeld. *Partial differential equation in physics*. 1949.

[43] P. Hohenberg and W. Kohn. “Inhomogeneous Electron Gas”. In: *Phys. Rev.* 136 (3B Nov. 1964), B864–B871. DOI: 10.1103/PhysRev.136.B864.

[44] W. Kohn and L. J. Sham. “Self-Consistent Equations Including Exchange and Correlation Effects”. In: *Phys. Rev.* 140 (4A Nov. 1965), A1133–A1138. DOI: 10.1103/PhysRev.140.A1133.

[45] Olga S. Bokareva et al. “Tuning Range-Separated Density Functional Theory for Photocatalytic Water Splitting Systems”. In: *Journal of Chemical Theory and Computation* 11.4 (Apr. 14, 2015), pp. 1700–1709. DOI: 10.1021/acs.jctc.5b00068.

[46] Gilbert Grell et al. “Multi-reference approach to the calculation of photoelectron spectra including spin-orbit coupling”. In: *J. Chem. Phys.* 143.7, 074104 (2015). DOI: http://dx.doi.org/10.1063/1.4928511.

[47] Iann C. Gerber and János G. Ángyán. “Potential curves for alkaline-earth dimers by density functional theory with long-range correlation corrections”. In: *Chemical Physics Letters* 416.4–6 (2005), pp. 370–375. DOI: http://dx.doi.org/10.1016/j.cplett.2005.09.059.

[48] Iann C. Gerber and János G. Ángyán. “Hybrid functional with separated range”. In: *Chemical Physics Letters* 415.1–3 (2005), pp. 100–105. DOI: http://dx.doi.org/10.1016/j.cplett.2005.08.060.

[49] Saumitra Saha et al. “Coexistence of 1,3-butadiene conformers in ionization energies and Dyson orbitals”. In: *The Journal of Chemical Physics* 123.12, 124315 (2005). DOI: http://dx.doi.org/10.1063/1.2034467.

[50] Alejandro Soba et al. “Real-space density functional theory and time dependent density functional theory using finite/infinite element methods”. In: *Computer Physics Communications* 183.12 (Dec. 2012), pp. 2581–2588. DOI: 10.1016/j.cpc.2012.07.007.

[51] Peter Bettess and Richard A. Abram. “Finite and infinite elements for a simple problem in quantum mechanics”. In: *Communications in numerical methods in engineering* 18.5 (2002), pp. 325–334.

[52] M. Valiev et al. “NWChem: A comprehensive and scalable open-source solution for large scale molecular simulations”. In: *Comput. Phys. Commun.* 181.9 (2010), pp. 1477–1489. DOI: http://dx.doi.org/10.1016/j.cpc.2010.04.018.

[53] M. J. Frisch et al. *Gaussian 09 Revision E.01*. Gaussian Inc. Wallingford CT 2009.

[54] B. S. Kirk et al. “libMesh: A C++ Library for Parallel Adaptive Mesh Refinement/Coarsening Simulations”. In: *Engineering with Computers* 22.3–4 (2006). http://dx.doi.org/10.1007/s00366-006-0049-3, pp. 237–254.

[55] Vicente Hernandez, Jose E. Roman, and Vicente Vidal. “SLEPc: A scalable and flexible toolkit for the solution of eigenvalue problems”. In: *ACM Trans. Math. Software* 31.3 (2005), pp. 351–362.

[56] V. Hernandez, J. E. Roman, and V. Vidal. "SLEPc: Scalable Library for Eigenvalue Problem Computations". In: *Lect. Notes Comput. Sci.* 2565 (2003), pp. 377–391.

[57] Satish Balay et al. *PETSc Web page*. http://www.mcs.anl.gov/petsc. 2016.

[58] Stephan Hüfner. *Photoelectron Spectroscopy*. 3rd ed. Berlin: Springer Verlag, 2003.

[59] C.J. Milne, T.J. Penfold, and M. Chergui. "Recent experimental and theoretical developments in time-resolved X-ray spectroscopies". In: *Coordination Chemistry Reviews* 277-278 (Oct. 2014), pp. 44–68. DOI: 10.1016/j.ccr.2014.02.013.

[60] A W Potts et al. "An experimental and theoretical study of the valence shell photoelectron spectra of purine and pyrimidine molecules". In: *J Phys. B-A. Mol. Opt.* 36.14 (2003), p. 3129.

[61] W.G. Richards. "The use of Koopmans' Theorem in the interpretation of photoelectron spectra". In: *International Journal of Mass Spectrometry and Ion Physics* 2.6 (1969), pp. 419–424. DOI: http://dx.doi.org/10.1016/0020-7381(69)80040-9.

[62] Anthony R. Schwager, Kevin H. Bell, and Ellak I. von Nagy-Felsobuki. "PHOTOELECTRON SPECTRA OF THE ALKYL PHENYL DISULFIDES". In: *Phosphorus, Sulfur, and Silicon and the Related Elements* 70.1 (1992), pp. 287–295. DOI: 10.1080/10426509208049177. eprint: http://dx.doi.org/10.1080/10426509208049177.

[63] David A. Egger et al. "Outer-valence Electron Spectra of Prototypical Aromatic Heterocycles from an Optimally Tuned Range-Separated Hybrid Functional". In: *JCTC* 10.5 (2014). PMID: 24839410, pp. 1934–1952. DOI: 10.1021/ct400956h.

[64] Diana Yepes et al. "Photoemission Spectra and Density Functional Theory Calculations of 3d Transition Metal–Aqua Complexes (Ti–Cu) in Aqueous Solution". In: *The Journal of Physical Chemistry B* 118.24 (2014). PMID: 24902000, pp. 6850–6863. DOI: 10.1021/jp5012389.

[65] J. Schirmer et al. "Strong correlation effects in the ionisation of CS2". In: *Chem. Phys. Lett.* 61.1 (1979), pp. 30–35. DOI: http://dx.doi.org/10.1016/0009-2614(79)85078-2.

[66] Leo P. Kadanoff and Gordon Baym. *Quantum Statistical Mechanics: Green's Function Method in Equilibrium and Nonequilibrium Problems*. Addison-Wesley Publishing Co. Inc., 1989.

[67] W. Von Niessen, J. Schirmer, and L. S. Cederbaum. "Computational methods for the one-particle green's function". In: *Computer Physics Reports* 1.2 (1984), pp. 57–125.

[68] Craig A. Bayse and Kristine N. Ortwine. "Calculation of Photoelectron Spectra of Molybdenum and Tungsten Complexes Using Green's Functions Methods". In: *The Journal of Physical Chemistry A* 111.32 (2007). PMID: 17636964, pp. 7841–7847. DOI: 10.1021/jp063029j. eprint: http://dx.doi.org/10.1021/jp063029j.

[69] J. Schirmer, L. S. Cederbaum, and O. Walter. "New approach to the one-particle Green's function for finite Fermi systems". In: *Phys. Rev. A* 28 (3 Sept. 1983), pp. 1237–1259. DOI: 10.1103/PhysRevA.28.1237.

[70] Yu Yan and M. J. Seaton. "R-matrix theory of the hydrogen atom". In: *Journal of Physics B: Atomic and Molecular Physics* 18.13 (1985), p. 2577.

[71] M J Seaton. "Use of the R matrix method for bound-state calculations. I. General theory". In: *Journal of Physics B: Atomic and Molecular Physics* 18.11 (1985), p. 2111.

[72] A.G. Sunderland et al. "A parallel R-matrix program PRMAT for electron–atom and electron–ion scattering calculations". In: *Comput. Phys. Commun.* 145.3 (2002), pp. 311–340. DOI: http://dx.doi.org/10.1016/S0010-4655(02)00140-6.

[73] L. Journel et al. "First experimental determination and theoretical calculation of partial photoionization cross sections of lithium over the energy region of hollow Atomic States". In: *Physical review letters* 76.1 (1996), p. 30.

[74] S. Diehl et al. "Angle-Resolved Photoelectron Spectrometry Studies of the Autoionization of the 2 s 2 2 p 2 P Triply Excited State of Atomic Lithium". In: *Physical review letters* 84.8 (2000), p. 1677.

[75] L. M. Kiernan et al. "Resonant photoionization of atomic lithium in the region of the first and second inner-shell thresholds". In: *J Phys. B-A. Mol. Opt.* 29.6 (1996), p. L181.

[76] B.D. Buckley, P.G. Burke, and Vo Ky Lan. "R-matrix calculations for electron-molecule scattering". In: *Computer Physics Communications* 17.1 (1979), pp. 175–179. DOI: http://dx.doi.org/10.1016/0010-4655(79)90080-8.

[77] B M McLaughlin and R C Forrey. "Low energy electron collisions with the N 2 H radical". In: *Journal of Physics: Conference Series* 388.5 (2012), p. 052027.

[78] Keith H. Johnson. "Scattered-Wave Theory of the Chemical Bond*". In: Advances in Quantum Chemistry 7 (1973). Ed. by Per-Olov Löwdin, pp. 143–185. DOI: http://dx.doi.org/10.1016/S0065-3276(08)60561-4.

[79] J. C. Slater and K. H. Johnson. "Self-Consistent-Field $X\alpha$ Cluster Method for Polyatomic Molecules and Solids". In: *Phys. Rev. B* 5 (3 Feb. 1972), pp. 844–853. DOI: 10.1103/PhysRevB.5.844.

[80] F Beleznay and M J Lawrence. "The 'muffin-tin' approximation in the calculation of electronic band structure". In: *Journal of Physics C: Solid State Physics* 1.5 (1968), p. 1288.

[81] D. D. Koelling, A. J. Freeman, and F. M. Mueller. "Shifts in the Electronic Band Structure of Metals Due to Non-Muffin-Tin Potentials". In: *Phys. Rev. B* 1 (4 Feb. 1970), pp. 1318–1324. DOI: 10.1103/PhysRevB.1.1318.

[82] M. Venut, M. Stener, and P. Decleva. "Valence photoionization of C6H6 by the B-spline one-centre expansion density functional method". In: *Chemical Physics* 234.1 (1998), pp. 95–109. DOI: http://dx.doi.org/10.1016/S0301-0104(98)00179-7.

[83] J. A. Richards and F. P. Larkins. "Molecular photoionisation calculations with numerical continuum wavefunctions: application to the hydrogen molecule". In: *Journal of Physics B: Atomic and Molecular Physics* 17.6 (1984), p. 1015.

[84] Thomas-C. Jagau and Anna I. Krylov. "Complex Absorbing Potential Equation-of-Motion Coupled-Cluster Method Yields Smooth and Internally Consistent Potential Energy Surfaces and Lifetimes for Molecular Resonances". In: *JPCL* 5.17 (Sept. 4, 2014), pp. 3078–3085. DOI: 10.1021/jz501515j.

[85] S. Bauch, L. K. Sørensen, and L. B. Madsen. "Time-dependent generalized-active-space configuration-interaction approach to photoionization dynamics of atoms and molecules". In: *Phys. Rev. A* 90.6 (Dec. 9, 2014). DOI: 10.1103/PhysRevA.90.062508.

[86] Liang Tao, C. W. McCurdy, and T. N. Rescigno. "Grid-based methods for diatomic quantum scattering problems: A finite-element discrete-variable representation in prolate spheroidal coordinates". In: *Phys. Rev. A* 79 (1 Jan. 2009), p. 012719. DOI: 10.1103/PhysRevA.79.012719.

[87] Zhigang Sun, Nanquan Lou, and Gunnar Nyman. "Time-Dependent Wave Packet Split Operator Calculations on a Three-Dimensional Fourier Grid in Radau Coordinates Applied to the OClO Photoelectron Spectrum". In: *The Journal of Physical Chemistry A* 108.42 (2004), pp. 9226–9232. DOI: 10.1021/jp0477203. eprint: http://dx.doi.org/10.1021/jp0477203.

[88] Gireesh M. Krishnan, Subhas Ghosal, and Susanta Mahapatra. "Theoretical Study of the Electronic Nonadiabatic Transitions in the Photoelectron Spectroscopy of F2O". In: *The Journal of Physical Chemistry A* 110.3 (2006). PMID: 16420003, pp. 1022–1030. DOI: 10.1021/jp0543882. eprint: http://dx.doi.org/10.1021/jp0543882.

[89] Russell T Pack and Gregory A. Parker. "Quantum reactive scattering in three dimensions using hyperspherical (APH) coordinates. Theory". In: *The Journal of Chemical Physics* 87.7 (1987), pp. 3888–3921. DOI: http://dx.doi.org/10.1063/1.452944.

[90] F. L. Yip, C. W. McCurdy, and T. N. Rescigno. "Hybrid orbital and numerical grid representation for electronic continuum processes: Double photoionization of atomic beryllium". In: *Phys. Rev. A* 81 (5 May 2010), p. 053407. DOI: 10.1103/PhysRevA.81.053407.

[91] H. R. Larsson et al. "Correlation effects in strong-field ionization of heteronuclear diatomic molecules". In: *Phys. Rev. A* 93 (1 Jan. 2016), p. 013426. DOI: 10.1103/PhysRevA.93.013426.

[92] O. V. Gritsenko and E. J. Baerends. "Time-dependent Dyson orbital theory". In: *Phys. Chem. Chem. Phys.* (2016). DOI: 10.1039/C6CP00888G.

[93] Aurora Ponzi et al. "Dynamical photoionization observables of the CS molecule: The role of electron correlation". In: *The Journal of Chemical Physics* 140.20, 204304 (2014). DOI: http://dx.doi.org/10.1063/1.4876495.

[94] Teijo Åberg. "Theory of X-Ray Satellites". In: *Phys. Rev.* 156 (1 Apr. 1967), pp. 35–41. DOI: 10.1103/PhysRev.156.35.

[95] Eric L. Michelsen. *Quirky Quantum Concepts*. Springer, 2014. DOI: 10.1007/978-1-4614-9305-1.

[96] K. Gokhberg et al. "Molecular photoionization cross sections by Stieltjes–Chebyshev moment theory applied to Lanczos pseudospectra". In: *J. Chem. Phys.* 130.6, 064104 (2009). DOI: http://dx.doi.org/10.1063/1.3073821.

[97] P.W. Langhoff. "Bounds for second-order optical properties from quantum-mechanical sum rules and the theory of moments". In: *Chemical Physics Letters* 9.2 (1971), pp. 89–94. DOI: http://dx.doi.org/10.1016/0009-2614(71)80193-8.

[98] P.W. Langhoff. "Stieltjes imaging of atomic and molecular photoabsorption profiles". In: *Chem. Phys. Lett.* 22.1 (1973), pp. 60–64. DOI: http://dx.doi.org/10.1016/0009-2614(73)80534-2.

[99] P. W. Langhoff et al. "Moment-theory investigations of photoabsorption and dispersion profiles in atoms and ions". In: *Phys. Rev. A* 14 (3 Sept. 1976), pp. 1042–1056. DOI: 10.1103/PhysRevA.14.1042.

[100] Liang Gong et al. "Numerical analysis on quantum dots-in-a-well structures by finite difference method". In: *Superlattices and Microstructures* 60 (2013), pp. 311–319. DOI: http://dx.doi.org/10.1016/j.spmi.2013.05.012.

[101] Liang Gong et al. "Numerical computation of pyramidal quantum dots with band non-parabolicity". In: *Superlattices and Microstructures* 61 (2013), pp. 81–90. DOI: http://dx.doi.org/10.1016/j.spmi.2013.06.011.

[102] I.K. Gainullin and M.A. Sonkin. "High-performance parallel solver for 3D time-dependent Schrodinger equation for large-scale nanosystems". In: *Computer Physics Communications* 188 (2015), pp. 68–75. DOI: http://dx.doi.org/10.1016/j.cpc.2014.11.005.

[103] Sang-Kil Son. "Voronoi-cell finite difference method for accurate electronic structure calculation of polyatomic molecules on unstructured grids". In: *Journal of Computational Physics* 230.5 (2011), pp. 2160–2173. DOI: http://dx.doi.org/10.1016/j.jcp.2010.12.012.

[104] Franz Aurenhammer. "Voronoi Diagrams& Mdash;a Survey of a Fundamental Geometric Data Structure". In: *ACM Comput. Surv.* 23.3 (Sept. 1991), pp. 345–405. DOI: 10.1145/116873.116880.

[105] N. Sukumar. "Voronoi cell finite difference method for the diffusion operator on arbitrary unstructured grids". In: *International Journal for Numerical Methods in Engineering* 57.1 (2003), pp. 1–34.

[106] Qiang Du and Max Gunzburger. "Grid generation and optimization based on centroidal Voronoi tessellations". In: *Applied Mathematics and Computation* 133.2–3 (2002), pp. 591–607. DOI: http://dx.doi.org/10.1016/S0096-3003(01)00260-0.

[107] Sang-Kil Son and Shih-I Chu. "Theoretical study of orientation-dependent multiphoton ionization of polyatomic molecules in intense ultrashort laser fields: A new time-dependent Voronoi-cell finite difference method". In: *Chem. Phys.* 366.1–3 (2009), pp. 91–102. DOI: http://dx.doi.org/10.1016/j.chemphys.2009.09.006.

[108] B. Shizgal. *Spectral Methods in Chemistry and Physics. Applications to Kinetic Theory and Quantum Mechanics*. 2nd ed. Springer Verlag, 2015.

[109] Joseph B. Fourier. *Theorie Analytique de la Chaleur*. Firmin Didot, 1822.

[110] Bengt Fornberg. *A Practical Guide to Pseudospectral Methods*. Ed. by P. G. Ciarlet et al. Vol. 1. Cambridge University Press, 1996.

[111] David J. Tannor. *Introduction to Quantum Mechanics. A Time-dependent Perspective*. Sausalito, California: University Science Book, 2007.

[112] Dequan Yu, Shu-Lin Cong, and Zhigang Sun. "An improved Lobatto discrete variable representation by a phase optimisation and variable mapping method". In: *Chem. Phys.* 458 (2015), pp. 41–51. DOI: http://dx.doi.org/10.1016/j.chemphys.2015.07.009.

[113] Liang-You Peng and Anthony F. Starace. "Application of Coulomb wave function discrete variable representation to atomic systems in strong laser fields". In: *JCP* 125.15, 154311 (2006).

[114] A. R. Edmonds. *Angular Momentum in Quantum Mechanics*. 4th ed. Princeton, New Jersey: Princeton University Press, 1996.

[115] Akbar Mohebbi, Mostafa Abbaszadeh, and Mehdi Dehghan. "The use of a meshless technique based on collocation and radial basis functions for solving the time fractional nonlinear Schrödinger equation arising in quantum mechanics". In: *Engineering Analysis with Boundary Elements* 37.2 (2013), pp. 475–485. DOI: http://dx.doi.org/10.1016/j.enganabound.2012.12.002.

[116] Lihua Wang, Fuyun Chu, and Zheng Zhong. "Study of radial basis collocation method for wave propagation". In: *Engineering Analysis with Boundary Elements* 37.2 (2013), pp. 453–463. DOI: http://dx.doi.org/10.1016/j.enganabound.2012.12.001.

[117] Richard Franke. "Scattered data interpolation: tests of some methods". In: *Math. Comp.* 38.157 (1982), pp. 181–200. DOI: 10.2307/2007474.

[118] J. C. Carr, W. R. Fright, and R. K. Beatson. "Surface interpolation with radial basis functions for medical imaging". In: *IEEE Transactions on Medical Imaging* 16.1 (Feb. 1997), pp. 96–107. DOI: 10.1109/42.552059.

[119] P. F. Batcho. "Computational method for general multicenter electronic structure calculations". In: *Phys. Rev. E* 61 (6 June 2000), pp. 7169–7183. DOI: 10.1103/PhysRevE.61.7169.

[120] S. Petersen, D. Dreyer, and O. von Estorff. "Practical considerations of the acoustic FEM for higher frequencies." In: *30. Tagung der Arbeitsgemeinschaft für Akustik DAGA 2004*. mubve. Straßburg, 2004, pp. 307–308.

[121] David A. Mazziotti. "Spectral difference methods for solving differential equations". In: *Chem. Phys. Lett.* 299.5 (1999), pp. 473–480. DOI: http://dx.doi.org/10.1016/S0009-2614(98)01324-4.

[122] C. Liang, R. Kannan, and Z.J. Wang. "A p-multigrid spectral difference method with explicit and implicit smoothers on unstructured triangular grids". In: *Computers & Fluids* 38.2 (2009), pp. 254–265. DOI: http://dx.doi.org/10.1016/j.compfluid.2008.02.004.

[123] Yen Liu, Marcel Vinokur, and Z.J. Wang. "Spectral difference method for unstructured grids I: Basic formulation". In: *Journal of Computational Physics* 216.2 (2006), pp. 780–801. DOI: http://dx.doi.org/10.1016/j.jcp.2006.01.024.

[124] Michael W. Frazier. *An Introduction to Wavelets Through Linear Algebra*. New York: Springer, 1999.

[125] Stephan Dahlke. "Wavelets: Construction Principles and Applications to the Numerical Treatment of Operator Equations". PhD thesis. Germany: RWTH Aachen, 1996.

[126] T. Torsti et al. "Three real-space discretization techniques in electronic structure calculation". In: *Physica Status Solidi (B)* 243.5 (2006), pp. 1016–1053. DOI: 10.1002/pssb.200541348.

[127] *Information technology – JPEG 2000 image coding system: Conformance testing*. Standard. International Organization for Standardization, Dec. 2004.

[128] Gerlind Plonka and Manfred Tasche. "On the Computation of Periodic Spline Wavelets". In: *Appl. Comput. Harmonic Anal. 2* 2.1 (1995), pp. 1–14. DOI: http://dx.doi.org/10.1006/acha.1995.1001.

[129] Marcílio N Guimarães and Frederico V Prudente. "A study of the confined hydrogen atom using the finite element method". In: *J Phys. B-A. Mol. Opt.* 38.15 (2005), p. 2811.

[130] Dong Xu, Jernej Stare, and Andrew L. Cooksy. "Solving the vibrational Schrödinger equation on an arbitrary multidimensional potential energy surface by the finite element method". In: *Comput. Phys. Commun.* 180.11 (2009), pp. 2079–2094. DOI: http://dx.doi.org/10.1016/j.cpc.2009.06.010.

[131] R. Alizadegan, K. J. Hsia, and T. J. Martinez. "A divide and conquer real space finite-element Hartree–Fock method". In: *J. Chem. Phys.* 132.3, 034101 (2010). DOI: http://dx.doi.org/10.1063/1.3290949.

[132] Jun Fang, Xingyu Gao, and Aihui Zhou. "A Kohn–Sham equation solver based on hexahedral finite elements". In: *Journal of Computational Physics* 231.8 (2012), pp. 3166–3180. DOI: http://dx.doi.org/10.1016/j.jcp.2011.12.043.

[133] W. Bangerth et al. "The deal.II Library, Version 8.4". In: *Journal of Numerical Mathematics* 24 (2016).

[134] F. Hecht. "New development in FreeFem++". In: *J. Numer. Math.* 20.3-4 (2012), pp. 251–265.

[135] Pavel Karban et al. "Numerical solution of coupled problems using code Agros2D". In: *Computing* 95.1 (2013), pp. 381–408. DOI: 10.1007/s00607-013-0294-4.

[136] B. Patzák. "OOFEM - an object-oriented simulation tool for advanced modeling of materials and structures". In: *Acta Polytechnica* 52.6 (2012), pp. 59–66.

[137] C. Perdigou and B. Audoly. "The viscous curtain: General formulation and finite-element solution for the stability of flowing viscous sheets". In: *Journal of the Mechanics and Physics of Solids* 96 (2016), pp. 291–311. DOI: http://dx.doi.org/10.1016/j.jmps.2016.07.015.

[138] F. Ballarin et al. "Fast simulations of patient-specific haemodynamics of coronary artery bypass grafts based on a POD-Galerkin method and a vascular shape parametrization". In: *Journal of Computational Physics* 315 (June 2016), pp. 609–628.

[139] H. Huang and B. W. Spencer. "Grizzly model of fully coupled heat transfer, moisture diffusion, alkali-silica reaction and fracturing processes in concrete". In: *Proceedings of the 9th International Conference on Fracture Mechanics of Concrete and Concrete Structures (FraMCoS-9), Berkeley, CA*. Ed. by V. Saouma, J. Bolander, and E. Landis. Paper 194, http://dx.doi.org/10.21012/FC9.194. May 2016.

[140] M. P. Lüthi et al. "Heat sources within the Greenland Ice Sheet: dissipation, temperate paleo-firn and cryo-hydrologic warming". In: *The Cryosphere* 9.1 (2015), pp. 245–253. DOI: 10.5194/tc-9-245-2015.

[141] P. Bauman, J. Jagodzinski, and B. S. Kirk. "Statistical calibration of thermocouple gauges used for inferring heat flux". In: *42nd AIAA Thermophysics Conference, Fluid Dynamics and Co-located Conferences*. http://dx.doi.org/10.2514/6.2011-3779. June 2011.

[142] Kyle A. Gamble et al. "A feasibility study on the use of the MOOSE computational framework to simulate three-dimensional deformation of CANDU reactor fuel elements". In: *Nuclear Engineering and Design* 293 (2015), pp. 385–394. DOI: http://dx.doi.org/10.1016/j.nucengdes.2015.07.028.

[143] Xianfeng Yang et al. "Fluid–structure interaction analysis of the drop impact test for helicopter fuel tank". In: *SpringerPlus* 5.1 (2016), p. 1573. DOI: 10.1186/s40064-016-3040-5.

[144] Jörg Ackermann. "Finite-element-method expectation values for correlated two-electron wave functions". In: *Phys. Rev. A* 52 (3 Sept. 1995), pp. 1968–1975. DOI: 10.1103/PhysRevA.52.1968.

[145] Armin Scrinzi. "A 3-dimensional finite elements procedure for quantum mechanical applications". In: *Comput. Phys. Commun.* 86.1 (1995), pp. 67–80. DOI: http://dx.doi.org/10.1016/0010-4655(94)00160-4.

[146] J.J. Soares Neto and Jan Linderberg. "A numerical study of various finite-element method schemes applied to quantum mechanical calculations". In: *Comput. Phys. Commun.* 66.1 (1991), pp. 55–65. DOI: http://dx.doi.org/10.1016/0010-4655(91)90007-8.

[147] Weiying Zheng, Lung-an Ying, and Peizhu Ding. "Numerical solutions of the Schrödinger equation for the ground lithium by the finite element method". In: *Appl. Math. Comput.* 153.3 (2004), pp. 685–695. DOI: http://dx.doi.org/10.1016/S0096-3003(03)00664-7.

[148] J. Ackermann, B. Erdmann, and R. Roitzsch. "A self-adaptive multilevel finite element method for the stationary Schrödinger equation in three space dimensions". In: *J. Chem. Phys.* 101.9 (1994), pp. 7643–7650. DOI: http://dx.doi.org/10.1063/1.468257.

[149] J. E. Pask et al. "Real-space local polynomial basis for solid-state electronic-structure calculations: A finite-element approach". In: *Phys. Rev. B* 59 (19 May 1999), pp. 12352–12358. DOI: 10.1103/PhysRevB.59.12352.

[150] Jan Linderberg. "Finite element methods in quantum mechanics". In: *Computer Physics Reports* 6.1 (1987), pp. 209–242. DOI: http://dx.doi.org/10.1016/0167-7977(87)90013-X.

[151] Lauri Lehtovaara, Ville Havu, and Martti Puska. "All-electron density functional theory and time-dependent density functional theory with high-order finite elements". In: *J. Chem. Phys.* 131.5, 054103 (2009). DOI: http://dx.doi.org/10.1063/1.3176508.

[152] P. Motamarri et al. "Higher-order adaptive finite-element methods for Kohn–Sham density functional theory". In: *Journal of Computational Physics* 253 (2013), pp. 308–343. DOI: http://dx.doi.org/10.1016/j.jcp.2013.06.042.

[153] E. Romero and J. E. Roman. "A parallel implementation of Davidson methods for large-scale eigenvalue problems in SLEPc". In: *ACM Trans. Math. Software* 40.2 (2014), 13:1–13:29. DOI: 10.1145/2543696.

[154] V. Hernandez, J.E. Roman, and A. Tomas. "Parallel Arnoldi eigensolvers with enhanced scalability via global communications rearrangement". In: *Parallel Computing* 33.7–8 (2007), pp. 521–540. DOI: http://dx.doi.org/10.1016/j.parco.2007.04.004.

[155] Joseph M. Elble, Nikolaos V. Sahinidis, and Panagiotis Vouzis. "GPU computing with Kaczmarz's and other iterative algorithms for linear systems". In: *Parallel Computing* 36.5–6 (2010). Parallel Matrix Algorithms and Applications, pp. 215–231. DOI: http://dx.doi.org/10.1016/j.parco.2009.12.003.

[156] Filipp Furche et al. "Accelerating molecular property calculations with nonorthonormal Krylov space methods". In: *The Journal of Chemical Physics* 144.17, 174105 (2016). DOI: http://dx.doi.org/10.1063/1.4947245.

[157] Siu-Wing Cheng and Jonathan Dey Tamal K.and Shewchuk. *Delaunay Mesh Generation*. 1st ed. Taylor & Francis, 2012.

[158] V.I. Lebedev and D.N. Laikov. "A quadrature formula for the sphere of the 131stalgebraic order of accuracy". In: *Doklady Mathematics* 59.3 (1999), pp. 477–481.

[159] Robert S. Womersley and Ian H. Sloan. "How good can polynomial interpolation on the sphere be?" In: *Advances in Computational Mathematics* 14.3 (2001), pp. 195–226. DOI: 10.1023/A:1016630227163.

[160] Ian H. Sloan and Robert S. Womersley. "Good approximation on the sphere, with application to geodesy and the scattering of sound". In: *Journal of Computational and Applied Mathematics* 149.1 (2002). Scientific and Engineering Computations for the 21st Century - Me thodologies and Applications Proceedings of the 15th Toyota Conference, pp. 227–237. DOI: http://dx.doi.org/10.1016/S0377-0427(02)00532-0.

[161] Thomas-C. Jagau et al. "A Fresh Look at Resonances and Complex Absorbing Potentials: Density Matrix-Based Approach". In: *JPCL* 5.2 (Jan. 16, 2014), pp. 310–315. DOI: 10.1021/jz402482a.

[162] Bjorn Engquist and Andrew Majda. "Absorbing boundary conditions for the numerical simulation of waves". In: *Math. Comp.* 31.0436612 (1977), pp. 629–651.

[163] Steffen Marburg and Bodo Nolte, eds. *Computational Acoustics of Noise Propagation in Fluids - Finite and Boundary Element Methods*. Springer, 2008.

[164] Francis Collino. "Perfectly Matched Absorbing Layers for the Paraxial Equations". In: *Journal of Computational Physics* 131.1 (1997), pp. 164–180. DOI: http://dx.doi.org/10.1006/jcph.1996.5594.

[165] Chunxiong Zheng. "A perfectly matched layer approach to the nonlinear Schrödinger wave equations". In: *Journal of Computational Physics* 227.1 (2007), pp. 537–556. DOI: http://dx.doi.org/10.1016/j.jcp.2007.08.004.

[166] R. J. Astley. "FE mode-matching schemes for the exterior Helmholtz problem and their relationship to the FE-DtN approach". In: *Communications in Numerical Methods in Engineering* 12.4 (1996), pp. 257–267. DOI: 10.1002/(SICI)1099-0887(199604)12:4<257::AID-CNM977>3.0.CO;2-8.

[167] D.N. Dai. "An improved boundary element formulation for wave propagation problems". In: *Engineering Analysis with Boundary Elements* 10.4 (1992), pp. 277–281. DOI: http://dx.doi.org/10.1016/0955-7997(92)90140-3.

[168] Martin Costabel. "Principles of boundary element methods". In: *Computer Physics Reports* 6.1 (1987), pp. 243–274. DOI: http://dx.doi.org/10.1016/0167-7977(87)90014-1.

[169] Whye-Teong Ang. *A Beginner's Course in Boundary Element Methods*. Boca Raton, Florida: Universal Publishers, 2007.

[170] Santosh Kumar Rana and Amit Jena. "A BEM formulation of two dimensional steady state heat conduction in exchanger tubes of arbitrary cross sections". In: *International Journal of Heat and Mass Transfer* 106 (2017), pp. 195–211. DOI: http://dx.doi.org/10.1016/j.ijheatmasstransfer.2016.10.055.

[171] Y.P. Gong, C.Y. Dong, and X.C. Qin. "An isogeometric boundary element method for three dimensional potential problems". In: *Journal of Computational and Applied Mathematics* 313 (2017), pp. 454–468. DOI: http://dx.doi.org/10.1016/j.cam.2016.10.003.

[172] Haijun Wu et al. "A Fast Multipole Boundary Element Method for Three-Dimensional Half-Space Acoustic Wave Problems Over an Impedance Plane". In: *International Journal of Computational Methods* 12.01 (2015), p. 1350090. DOI: 10.1142/S0219876213500904

[173] F. Guarracino, V. Minutolo, and L. Nunziante. “A simple analysis of soil-structure interaction by BEM-FEM coupling”. In: *Engineering Analysis with Boundary Elements* 10.4 (1992), pp. 283–289. DOI: http://dx.doi.org/10.1016/0955-7997(92)90141-S.

[174] O. C. Zienkiewicz, D. W. Kelly, and P. Bettess. “The coupling of the finite element method and boundary solution procedures”. In: *International Journal for Numerical Methods in Engineering* 11.2 (1977), pp. 355–375. DOI: 10.1002/nme.1620110210.

[175] D. Dreyer and O. Von Estorff. “Improved conditioning of infinite elements for exterior acoustics”. In: *International Journal for Numerical Methods in Engineering* 58.6 (2003). 00049, pp. 933–953.

[176] J. E. Roman et al. *SLEPc Users Manual*. Tech. rep. DSIC-II/24/02 - Revision 3.7. D. Sistemes Informàtics i Computació, Universitat Politècnica de València, 2016.

[177] V. Hernandez et al. *A survey of software for sparse eigenvalue problems*. Tech. rep. STR-7. Available at http://slepc.upv.es. Universitat Politècnica de València, 2009.

[178] V. Hernandez et al. *A survey of software for sparse eigenvalue problems*. Tech. rep. STR-4. Available at http://slepc.upv.es. Universitat Politècnica de València, 2009.

[179] V. Hernandez et al. *A survey of software for sparse eigenvalue problems*. Tech. rep. STR-5. Available at http://slepc.upv.es. Universitat Politècnica de València, 2009.

[180] G. W. Stewart. “A Krylov–Schur Algorithm for Large Eigenproblems”. In: *SIAM Journal on Matrix Analysis and Applications* 23.3 (2002), pp. 601–614. DOI: 10.1137/S0895479800371529. eprint: http://dx.doi.org/10.1137/S0895479800371529.

[181] Wolfram Koch and Max C. Holthausen. *A Chemist’s Guide to Density Functional Theory*. 2nd ed. Wiley-VCH Verlag GmbH, 2001.

[182] R. Ditchfield, W. J. Hehre, and J. A. Pople. “SelfConsistent MolecularOrbital Methods. IX. An Extended GaussianType Basis for MolecularOrbital Studies of Organic Molecules”. In: *The Journal of Chemical Physics* 54.2 (1971), pp. 724–728. DOI: http://dx.doi.org/10.1063/1.1674902.

[183] G. A. Petersson et al. “A complete basis set model chemistry. I. The total energies of closedshell atoms and hydrides of the firstrow elements”. In: *The Journal of Chemical Physics* 89.4 (1988), pp. 2193–2218. DOI: http://dx.doi.org/10.1063/1.455064.

[184] Hisayoshi Iikura et al. “A long-range correction scheme for generalized-gradient-approximation exchange functionals”. In: *The Journal of Chemical Physics* 115.8 (2001), pp. 3540–3544. DOI: http://dx.doi.org/10.1063/1.1383587.

[185] Florian Weigend and Reinhart Ahlrichs. “Balanced basis sets of split valence, triple zeta valence and quadruple zeta valence quality for H to Rn: Design and assessment of accuracy”. In: *Phys. Chem. Chem. Phys.* 7 (18 2005), pp. 3297–3305. DOI: 10.1039/B508541A.

[186] Hang Si. “TetGen, a Delaunay-Based Quality Tetrahedral Mesh Generator”. In: *ACM Trans. Math. Softw.* 41.2 (Feb. 2015), 11:1–11:36. DOI: 10.1145/2629697.

[187] Hirofumi Tomita et al. “Shallow Water Model on a Modified Icosahedral Geodesic Grid by Using Spring Dynamics”. In: *Journal of Computational Physics* 174.2 (2001), pp. 579–613. DOI: http://dx.doi.org/10.1006/jcph.2001.6897.

[188] D. A. Randall et al. “Climate modeling with spherical geodesic grids”. In: *Computing in Science Engineering* 4.5 (Sept. 2002), pp. 32–41. DOI: 10.1109/MCISE.2002.1032427.

[189] Robert S. Womersley and Ian H. Sloan. “How good can polynomial interpolation on the sphere be?” In: *Advances in Computational Mathematics* 14.3 (2001), pp. 195–226. DOI: 10.1023/A:1016630227163.

[190] J Fliege and U Maier. “The distribution of points on the sphere and corresponding cubature formulae”. In: *IMA Journal of Numerical Analysis* 19.2 (1999), pp. 317–334. DOI: 10.1093/imanum/19.2.317. eprint: http://imajna.oxfordjournals.org/content/19/2/317.full.pdf+html.

[191] Mark A. Spackman. “Potential derived charges using a geodesic point selection scheme”. In: *Journal of Computational Chemistry* 17.1 (1996), pp. 1–18. DOI: 10.1002/(SICI)1096-987X(19960115)17:1<1::AID-JCC1>3.0.CO;2-V.

[192] Guo-Zhu Zhu and Lai-Sheng Wang. “Communication: Vibrationally resolved photoelectron spectroscopy of the tetracyanoquinodimethane (TCNQ) anion and accurate determination of the electron affinity of TCNQ”. In: *J. Chem. Phys.* 143.22, 221102 (2015). DOI: http://dx.doi.org/10.1063/1.4937761.

[193] J B West et al. “A high resolution angle resolved photoelectron spectroscopy study of N 2”. In: *Physica Scripta* 41.4 (1990), p. 487.

[194] Sunil R. Desai, Hongbin Wu, and Lai-Sheng Wang. “Vibrationally resolved photoelectron spectroscopy of AlO- and AlO2-”. In: *International Journal of Mass Spectrometry and Ion Processes* 159.1 (1996), pp. 75–80. DOI: http://dx.doi.org/10.1016/S0168-1176(96)04443-6.

[195] S. Alitalo et al. “The valence photoelectron satellite spectra of Kr and Xe”. In: *Journal of Electron Spectroscopy and Related Phenomena* 114-116 (2001). Proceeding of the Eight International Conference on Electronic Spectroscopy and Structure, pp. 141–146. DOI: http://dx.doi.org/10.1016/S0368-2048(00)00277-2.

[196] C.G. Ning et al. “Probing Dyson orbitals with Green’s Function theory and Electron Momentum Spectroscopy”. In: *Chem. Phys. Lett.* 421.1–3 (2006), pp. 52–57. DOI: http://dx.doi.org/10.1016/j.cplett.2006.01.040.

[197] S Krummacher et al. “Inner-shell photoemission studies of lithium and sodium vapour”. In: *Journal of Physics B: Atomic and Molecular Physics* 15.23 (1982), p. 4363.

[198] I. Reineck et al. “High-resolution UV photoelectron spectrum of CO2”. In: *Chemical Physics* 78.3 (1983), pp. 311–318. DOI: http://dx.doi.org/10.1016/0301-0104(83)85116-7.

[199] H. Veenhuizen et al. “High resolution angle-resolved photoelectron spectrum of CO2, excited with polarized resonance radiation”. In: *Journal of Electron Spectroscopy and Related Phenomena* 41.2 (1986), pp. 205–223. DOI: http://dx.doi.org/10.1016/0368-2048(86)85004-6.

[200] Lai-Sheng Wang et al. “High resolution UV photoelectron spectroscopy of CO+2, COS+ and CS+2 using supersonic molecular beams”. In: *Journal of Electron Spectroscopy and Related Phenomena* 47 (1988), pp. 167–186. DOI: http://dx.doi.org/10.1016/0368-2048(88)85010-2.

[201] C.R. Brundle and D.W. Turner. “Studies on the photoionisation of the linear triatomic molecules: N2O, COS, CS2 and CO2 using high-resolution photoelectron spectroscopy”. In: *International Journal of Mass Spectrometry and Ion Physics* 2.3 (1969), pp. 195–220. DOI: http://dx.doi.org/10.1016/0020-7381(69)80018-5.

[202] S.Y. Truong et al. “Threshold photoelectron spectroscopy of H2O and D2O over the photon energy range 12–40eV”. In: *Chemical Physics* 355.2 (Jan. 2009), pp. 183–193. DOI: 10.1016/j.chemphys.2008.12.009.

[203] L. Karlsson. “Isotopic and vibronic coupling effects in the valence electron spectra of H2 16O, H2 18O, and D2 16O”. In: *J. Chem. Phys.* 62.12 (1975), p. 4745. DOI: 10.1063/1.430423.

[204] C.G. Ning et al. “High resolution electron momentum spectroscopy of the valence orbitals of water”. In: *Chemical Physics* 343.1 (Jan. 2008), pp. 19–30. DOI: 10.1016/j.chemphys.2007.09.030.

# A | Appendix

## A.1 Delaunay Triangulation

The explicit setup of non-regular meshes for the use in finite element schemes is not trivial at all. There are however schemes available, among which are the Delaunay and Voronoi tesselations which are their respective dual schemes. Since in this thesis, only Delaunay tesselation is used, I will focus on this method and its properties only.
In mathematics one understands under a triangulation a connection of points to simplices. Thereby a structure is denoted as a simplex in $n$ dimensions, if has as few vertices as possible in this dimension. A simplex in $2D$ *e.g.* is a triangle while it is in $3D$ a tetrahedron. Moreover, a simplex is denoted as Delaunay simplex if there is a circumsphere such that no vertex is inside of this sphere.
A bit more intuitive acess to this scheme can be obtained via the Voronoi diagram: A Voronoi diagram splits a given volume (in $3D$) into elements using a set of points $p_i$ in this volume by assigning each point to the element of his nearest point $p_i$. Having this tesselation, one can transform it to a set of Delaunay simplices by connecting the points $p_i$ each with their direct neighbours [186].